PHASE STABILITY OF BETA-GALLIA RUTILE INTERGROWTHS

BY

ANDREA L. JAROMIN

A THESIS
SUBMITTED TO THE FACULTY OF

ALFRED UNIVERSITY

IN PARTIAL FULFILLMENT OF THE REQUIREMENTS
FOR THE DEGREE OF

MASTER OF SCIENCE

IN

MATERIALS SCIENCE & ENGINEERING

ALFRED, NEW YORK

APRIL, 2004

Alfred University theses are copyright protected and may be used for education or personal research only. Reproduction or distribution in part or whole is prohibited without written permission from the author.

PHASE STABILITY OF BETA-GALLIA RUTILE INTERGROWTHS

BY

ANDREA JAROMIN

B.S. ALFRED UNIVERSITY (2002)

SIGNATURE OF AUTHOR (Signature on file)

APPROVED BY (Signature on file)
DOREEN EDWARDS, ADVISOR

(Signature on file)
ALASTAIR CORMACK, ADVISORY COMMITTEE

(Signature on file)
SCOTT MISTURE, ADVISORY COMMITTEE

(Signature on file)
DOREEN EDWARDS, CHAIR, ORAL THESIS DEFENSE

ACCEPTED BY (Signature on file)
ALASTAIR CORMACK, DEAN,
SCHOOL OF ENGINEERING

ACKNOWLEDGMENTS

First and foremost, I would like to thank my advisor, Dr. Doreen Edwards, for being such a great person to work for. We've had engaging, thought-provoking conversations where I learned more than I could have learned from any textbook. She was also adamant on me reaching my goal of graduating in a year and a half, while still letting me explore my research on my own. We also had some great times outside of the office!

I would like to thank Dr. Alastair Cormack and Dr. Scott Misture for being so helpful as committee members, and most of all, for their understanding and speediness in reviewing my thesis. Without their extra help, I would have certainly been an August grad. Dr. Casper McConville also helped a great deal with my TEM work.

My office mates, Nate, Malin, Annette and Mike were of so much comfort at times, and were great people to have around to ask quick questions, and also to talk about important research concepts. I'd like to especially thank Nate for being so patient in answering my questions in Characterization, Kinetics and Thermo. Also, Malin was always smiling and enthusiastic about anything and everything we managed to talk about. I can only pray that I'll ever have great co-workers like them again someday.

I'd also like to thank everyone in BMH 116, Aladdin, Fab, Doug, Bryan, Jeurgen, and sometimes Dr. Matt, for letting me mooch off of your bagels, for tolerating my lab infractions and for listening to my chatter when I just needed a change of scenery. I'd also like to thank Dr. Clare, for not getting angry when I interrupted most her group meetings, and being so understanding when I blew up her microwave.

Outside the office, I'd like to thank my girls, Fabienne, Morgana, Liz and Jill for always being ready for a relaxing trip to the mall, or a night out to the *club*. I truly value all they've been through with me, including listening to my excuses for not going out, and then finally convincing me it was for my own good.

I'd also like to thank Nana's, for not only phenomenally tasty food, but for a place to sit with my buddies, to escape reality for awhile.

If it weren't for my father's love of math, and my mother's pushing me towards a non-traditional job for a female, I wouldn't be writing this today. They made me strong and ambitious. My parents have always listened to my babbling about technical stuff and school work when they didn't really know how to relate, but they always listened and kept me motivated.

Last, but not least, I'd like to thank my fiancé, Kevin Kazmierczak. I couldn't count the number of tears you've catched and hugs you've revived me with. You stuck with me through the cranky mornings after the all-nighters, boring homework-filled Friday nights and were always willing to go out of your way to help me when I didn't plan things very well. Your *madd* computer skills have rescued many a paper/lab report, and have patiently hooked up my computer for my defense presentation while I was busy running around. Congrats on all you've accomplished in your time here also, while continuously supporting me!

I couldn't have done it without all of you, and I really appreciate everything you've done for me over the years. Thanks!

TABLE OF CONTENTS

LIST OF TABLES

LIST OF FIGURES

Page

.

ABSTRACT

Beta-gallia rutile intergrowths are crystal structures consisting of a β-gallia component and a rutile-structured oxide component in the stoichiometry $Ga_4Mn_{n-4}O_{2n-2}$ where M is Ge, Sn or Ti, and $n \geq 5$. This structure is of interest as an ion-storage material due to the 2.5Å hexagonal tunnels suitable for the intercalation of small to medium sized cations such as Li^+. The purpose of this study was to attain low n-value intergrowths due to their higher tunnel density, using a reducible rutile-structured component.

Two systems were studied. The Ga_2O_3-Al_2O_3-TiO_2 system was studied because Ti^{4+} is reducible. Previous research showed that only higher n-value intergrowths were stable in the Ga_2O_3-TiO_2 system; therefore Al^{3+} was added in an attempt to stabilize lower n-value phases. Solid state synthesis at 1400ºC was used to prepare samples with the stoichiometry $Ga_{4-4x}Mn_{n-4}O_{2n-2}$ combinations of n ranging from 4 to 29 and x ranging from 0 to 1 and x-ray diffraction was used to characterize samples. Results show that while the addition of Al^{3+} decreases the cell volume of the β-gallia, pseudobrookite and corundum structures, it does not stabilize intergrowth structures with $n \leq 17$. For those samples prepared as n = 5, x = 0.1, 0.3, 0.5, 0.7, and 0.75, β-gallia and pseudobrookite were formed, while samples prepared as n = 5, x = 0.85, 0.90 and 1.0 corundum and pseudobrookite were formed and the sample prepared as n = 5, x = 0.80, was triphasic with corundum, pseudobrookite and β-gallia. Samples prepared as n = 7, 9, 15 and 17 with x = 0.1 and n = 9, x = 0 were biphasic with n = 17 intergrowth and pseudobrookite, whereas samples prepared with the same n-value and x = 0.5 contained pseudobrookite and n = 33 intergrowth. Samples prepared as n = 7, 9, 15, 17, 21 and 25, x = 0.3 were triphasic with pseudobrookite and n = 17 and n = 21 intergrowth. The sample prepared as n = 9, x = 0.9 contained rutile and pseudobrookite. Samples prepared as n = 15, 17, 19, 21, 23, 25 and 27, x = 0, n = 17, 25 and 27, x = 0.1, n = 25 and 29, x = 0.2 all contained phase pure intergrowths whereas n = 19, 21, x = 0 contained n = 21 intergrowth and the rest contained n = 33 intergrowth. The sample prepared as n = 25, x = 0.5 was triphasic with n = 33 intergrowth, rutile and pseudobrookite. The sample

prepared as n = 25, x = 0.7 was biphasic with pseudobrookite and rutile. An isothermal phase diagram is presented.

The Ga_2O_3-MnO_2 system was chosen because manganese, like Ti^{4+} is well-known as being reducible and is widely used in the battery industry. Hydrothermal synthesis was used to prepare samples with n = 5, 7 and 9, pH ranging from 0.7 to 9.8 with temperatures of 150º-235ºC and autogenic pressures. Samples were characterized with x-ray diffraction, thermal gravimetric analysis, differential scanning calorimetry and transmission electron microscopy. Results showed a strong correlation between pH, temperature and phases attained. Samples prepared with a pH < 7 contained diaspore as a major phase, and samples prepared as pH > 7 generally contained spinel as a major phase. Four samples prepared as n = 9 with pH > 9 and processing temperature less than 170ºC did not contain spinel but unknown major phases. One sample prepared as n = 9, pH = 6.6 and processing temperature of 225ºC contained rutile in addition to diaspore and one sample prepared as n = 9, pH = 8.7 and processing temperature of 230ºC contained bixbyite in addition to spinel. Unknown minor phases were a function of processing temperature. Analysis of thermal analysis data and x-ray diffraction after thermal events was able to yield possible transitions occurring in known major phases and was not able to determine the composition of the unknown major phases or transitions occurring.

1 Introduction

1.1 Background

Beta-gallia rutile intergrowths are the resulting crystal structures when β-Ga_2O_3 is reacted at high temperatures with a rutile-structure oxide in the stoichiometry $Ga_4M_{n-4}O_{2n-2}$, where M is Ge, Sn or Ti, and $n \geq 5$.[1] In an intergrowth structure, individual subunits of the components are 'intergrown,' where characteristics of the structure of each component are maintained. Figure 1.1 shows the structures of β-Ga_2O_3 and rutile, with darker and lighter shading, respectively, and the resulting intergrowth structures. These crystal structures are of interest because of the ~2.5Å hexagonal tunnels, which are suitable for small to medium sized cations such as Li^+. These crystal structures are being investigated as an energy storage material. Structures with similar tunnels have also been investigated for ion storage applications.[2-5] For example, γ-MnO_2 shows 2×1 and 1×1 tunnels and is an intergrowth of β-MnO_2 and ramsdellite-MnO_2, shown in Figure 1.2. Beta-gallia rutile intergrowths have potential benefits over other ion-storage materials. There are no bottlenecks in the structure which can hinder the migration of ions,[3] and they do not require the conducting ion to be inserted in order to stabilize the structure.[6]

Beta-gallia rutile intergrowths have been studied previously, as summarized in Table 1-I. For systems with germanium oxide as the rutile component, the n = 5 and n = 7 intergrowth structures have been found stable. Systems with titanium oxide as the rutile component have been studied extensively. The lowest stable n-value is n = 9, where $9 < n < 51$ (n is odd only) have been characterized. It is unknown why even n-value intergrowths do not form. Systems with tin oxide as the rutile component have been shown to be stable only for n = 5; however, the addition of In^{3+} into the β-gallia lattice will stabilize n = 6, and odd values between 7 and 17. This stabilization has been attributed to the reduction of the lattice mismatch resulting from the addition of larger In^{3+} for Ga^{3+}. This lattice mismatch can be calculated as a percentage difference between the b-parameter of the β-gallia component and the c-parameter of the rutile component, as shown in Table 1-I.

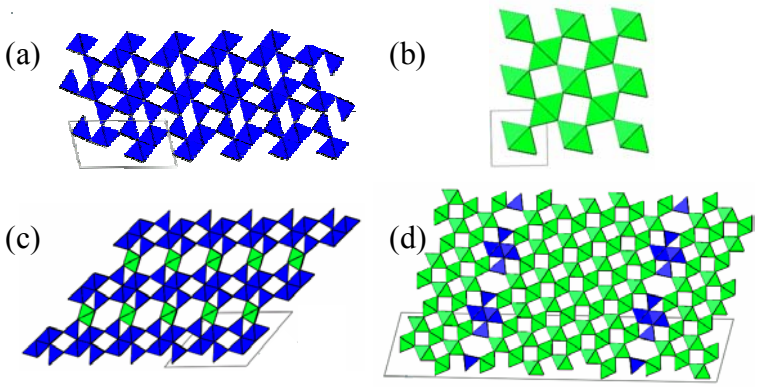

Figure 1.1. Crystal structures of (a) β-gallia structure (b) rutile structure (c) n = 5 β-gallia rutile intergrowth structure, (d) n = 25 β-gallia rutile intergrowth structure. Rutile is projected along the c axis and all others are projected along the b axis.

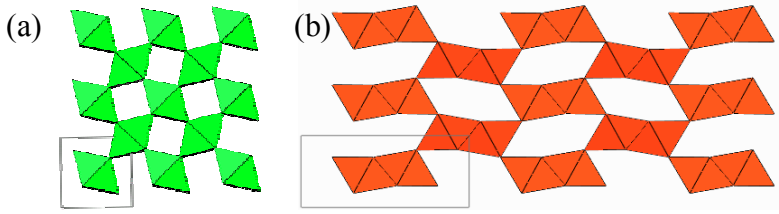

Figure 1.2. Crystal structures projected along the b-axis of (a) pyrolusite (rutile-structure) and (b) ramsdellite, where γ-MnO_2 is an intergrowth of these structures, forming 1×2 tunnels.

Table 1-I. Examples of β-Gallia Rutile Intergrowths.

β-gallia	$b_{\beta\text{-gallia}}$(Å)	Rutile	c_r(Å)	Lattice Mismatch[1]	Stable Intergrowths	Ref
Ga_2O_3	3.04	GeO_2	2.86	+0.06	n=5,7	7
Ga_2O_3	3.04	MnO_2	2.86	+0.06	This Study	-
Ga_2O_3	3.04	TiO_2	2.96	+0.03	n=9-51, odd n only	1,8,9
Ga_2O_3	3.04	SnO_2	3.19	-0.05	n=5	10
$Ga_{1.4}In_{0.6}O_3$	3.15	SnO_2	3.19	-0.01	n=6, 7-17, odd n only	11

[1] Lattice mismatch defined as $(b_\beta - c_r)/b_\beta$

1.2 Approach

The goal of this work was to prepare β-gallia rutile intergrowth structures with low n-values containing a reducible cation. A comparison of Figure 1.1(c) and Figure 1.1(d) demonstrates how the concentration of these hexagonal tunnels decreases with increasing n-value, where lower-n phases have higher tunnel density. A reducible cation is desirable because it is able to participate in Li-ion insertion reactions, such as:

$$Li + Ti^{4+} \rightarrow Li^{+} + Ti^{3+}$$

Two systems were chosen for investigation, the Ga_2O_3-Al_2O_3-TiO_2 system and the Ga_2O_3-MnO_2 system. The Ga_2O_3-Al_2O_3-TiO_2 system was chosen because Ti^{4+} is reducible; however, previous research showed that only higher n-value intergrowths were stable in the Ga_2O_3-TiO_2 system. The issue with this study was then stabilizing low n-value intergrowths. Because decreasing the lattice mismatch was shown to stabilize the Ga_2O_3-SnO_2 system and because the addition of Al^{3+} was reported to stabilize low n-value intergrowths in the Ga_2O_3-TiO_2 system,[1] Al^{3+} was selected as a means of reducing size of the β-gallia component. The processing method chosen was solid state synthesis, as this was used in previous research. Oxide powders were mixed, pressed into pellets, then heated to 1400ºC, until it was determined that equilibrium had been reached, often taking weeks of firing.

The Ga_2O_3-MnO_2 system was chosen for study because manganese is well-known as being reducible and is widely used in the battery industry. Because Mn^{4+} is unstable at low pO_2 pressures and high temperatures, hydrothermal synthesis was employed. This method involves the heating of reactants as a solution at elevated pressure and temperatures of 100º-374ºC. The method has recently gained interest as a means of decreasing processing time and cost and for the production of unique materials.

Because the background information and experimental procedures varied significantly in each system, this thesis is organized as two "stand-alone" manuscripts, presented in Chapters 2 and 3. Each chapter has its own introduction and experimental section, in addition to results and discussion. Chapter 4 further summarizes the work and provides recommendations for future research.

1.3 References

1. L.A. Bursill and G.G. Stone, "Tunnel and Intergrowth Structures in the Gallia-rich Gallium Titanate System," *J. Solid State Chem.,* **38** [1] 149-57 (1981).

2. S. Yoshikado, T. Ohachi, I. Taniguchi, M. Wantanabe, Y. Fujiki, and Y. Onoda, "Ion Conduction in One-Dimensional Ionic Conductors $A_{1-x}Ti_{2+x}B_{5-x}O_{12}$ (ATBO, A=Na or K and B=Al or Ga, x<1)," *Solid State Ionics,* **35** [3] 377-85 (1989).

3. M. Watanabe, T. Sasaki, Y. Kitami, and Y. Fujiki, "One-Dimensional Large Tunnels in the New Compound: $K_xGa_{16+x}Ti_{16-x}O_{56}$ (x<2)," *J. Solid State Chem.,* **68** [1] 177-80 (1987).

4. J. Desilvestro and O. Haas, "Metal Oxide Cathode Materials for Electrochemical Energy Storage: A Review," *J. Electrochem. Soc.,* **137** [1] 5C-19C (1990).

5. M.M. Thackeray, "Manganese Oxides for Lithium Batteries," *Prog. Solid State Chem.,* **25** [1] 1-71 (1997).

6. M. Wantanabe, Y. Fujiki, S. Yoshikado, and T. Ohachi, "Structural Aspects of the New One-Dimensional Ionic Conductors: $A_xGa_8Ga_{8+x}Ti_{16-x}O_{56}$ (A=K, Rb and Cs, x<2)," *Solid State Ionics,* **28-30** [1] 257-61 (1988).

7. A. Kahn, V. Agafonov, D. Michel, and M.P.Y. Jorba, "New Gallium Germanates with Tunnel Structures: α-Ga_4GeO_8 and $Ga_4Ge_3O_{12}$," *J. Solid State Chem.,* **65** [3] 377-82 (1986).

8. S. Kamiya and R.J.D. Tilley, "Phase Relations in the Pseudobinary System TiO_2-Ga_2O_3," *J. Solid State Chem.,* **22** [1] 205-16 (1977).

9. D.J. Lloyd, I.E. Grey, and L.A. Bursill, "The Structure of $Ga_4Ti_{21}O_{48}$," *Acta. Crystallogr.,* **32B** [11] 1756-61 (1975).

10. M.B. Varfolomeev, A.S. Mironova, T.I.Dudina, and N.D. Koldashov, "Interaction of Gallium (III) Oxide," *Zh. Neorg. Khim.,* **20** [6] 3140-41 (1975).

11. D. Edwards, T.O. Mason, W. Sinkler, L.D. Marks, K.R. Poeppelmeier, X. Hu, and J.D. Jorgensen, "Tunneled Intergrowth Structures in the Ga_2O_3-In_2O_3-SnO_2 System," *J. Solid State Chem.,* **150** [2] 294-304 (2000).

2 Phase Stability of Beta-Gallia Rutile Intergrowths

2.1 Introduction

Beta-gallia rutile intergrowths possess a β-gallia structure component, (monoclinic Ga_2O_3) and a rutile structure component, such as Sn, Ge, or Ti oxide in the ratio $Ga_4M_{n-4}O_{2n-2}$, as shown in Figure 2.1. These intergrowth structures possess hexagonal tunnels about 2.5Å in size along the [010] direction. Because of their size and alignment, these tunnels may be suitable for intercalation of small to medium sized cations.

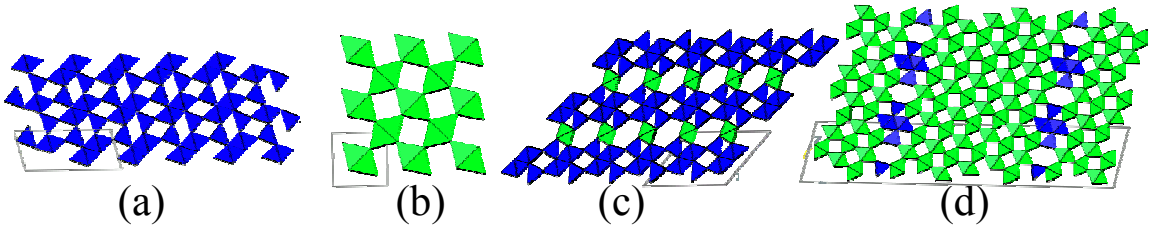

Figure 2.1. Crystal structures of (a) β-gallia structure (b) rutile structure (c) n = 5 β-gallia rutile intergrowth structure, (d) n = 25 β-gallia rutile intergrowth structure. The darker shading is β-gallia and the lighter shading is rutile.

The stability of β-gallia rutile intergrowths varies according to components. The system containing germanium dioxide as the rutile component forms intergrowths with n = 5 and 7[1], whereas the tin dioxide system forms an n = 5 intergrowth.[2] Lejus[3] studied the Ga_2O_3-TiO_2 system between 1100º-1600ºC and found the existence of a new phase rich in titanium, but was unable to determine its structure. Recurrent $(210)_R$ boundaries in intergrowths with $15 \leq n \leq 23$ odd were shown by Gibb and Anderson,[4] and the monoclinic C2/m space group was determined when the n = 25 structure was studied in detail by Lloyd et.al.[5] Kamiya and Tilley[6] found intergrowths of $11 \leq n \leq 29$ with n odd, to be stable at 1350ºC, with no evidence of the intermediate phase Ga_2TiO_5. Bursill and Stone[7] contradicted previous work by presenting the stability range for the intergrowth structure to be $9 \leq n \leq 21$ at 1300ºC, with an increase in stable phases to $5 \leq n \leq 50$ when the temperature was raised to 1500ºC. At 1400ºC, the highest stable intergrowth was found to be $n \cong 37$. Most significantly, they claimed that n = 9 was the lowest stable intergrowth, that n = 5 was metastable with respect to Ga_2TiO_5 and β-Ga_2O_3, and that

n = 7 was metastable with respect to Ga_2TiO_5 and n = 9. In the same study, it was claimed that replacement of Ga^{3+} by some Al^{3+} stabilized the n = 7 structure.

The Ga_2O_3-Al_2O_3 system shows solid solutions of β-Ga_2O_3 and α-Al_2O_3 (corundum), although there is disagreement on the solubility limits. Hill and Roy[8] reported the solubility of Al^{3+} in the β-Ga_2O_3 structure to be about 67% (cation basis) and the solubility of Ga^{3+} in α-Al_2O_3 to be around 25%. Mizuno et al[9] also studied this system, reporting the solubility limits of Al^{3+} in the β-Ga_2O_3 structure to be about 75% and the solubility limit of Ga^{3+} in α-Al_2O_3 to be 15%.

The Ga_2O_3-TiO_2 system has a line compound Ga_2TiO_5, having the pseudo-brookite structure with a space group Bbmm, which is isostructural to Al_2TiO_5 and Fe_2TiO_5.[10] The Al_2O_3-TiO_2[3,11,12] system has been studied thoroughly due to its significance in low thermal expansion applications. At 1400ºC, there exists a line compound β-Al_2TiO_5[11] with no evidence of a solid solution or other compounds. Ga_2TiO_5 is stable between 1300º-1580ºC whereas Al_2TiO_5 is stable between 1200º-1850ºC.[3]

In this work, the Ga_2O_3-Al_2O_3-TiO_2 system was investigated in an attempt to synthesize low n, titanium-containing intergrowths for ion-storage applications. Low n values are desired because of the higher tunnel densities and hence higher theoretical ion storage capacities. Selection of a titanium-containing intergrowth is desirable because titanium is easily reducible and can participate in an ion-storage reaction such as:

$$Li + Ti^{4+} \rightarrow Li^{+} + Ti^{3+}$$

Samples were prepared by solid state reaction to 1400ºC and characterized using x-ray diffraction. Aluminum substitution was not found to stabilize lower n-value intergrowths, but the work resulted in an isothermal sub-solidus phase diagram for the Ga_2O_3-Al_2O_3-TiO_2 system.

2.2 Experimental Procedure

Samples were prepared using the formula $Ga_{4-4x}Al_{4x}Ti_{n-4}O_{2n-2}$ with combinations with n ranging from 4 to 29 and x ranging from 0 to 1. Commercial oxide powders

(>99.9% purity on cation basis, Sigma-Aldrich Chemical Co.) were dried at 700ºC to remove water, weighed to ± 2% stoichiometry and then ground manually in an agate mortar and pestle. Samples were pressed into pellets at 50MPa, and placed into high purity alumina crucibles between sacrificial pellets and heated at 1100ºC overnight. They were re-crushed then repressed and heated to 1400ºC between 7 and 23 days, until the samples were phase pure, or until it was apparent that equilibrium was reached.

X-ray powder diffraction was carried out on a Phillips XRG3100 diffractometer using Cu Kα radiation (40kV, 20mA). The scan parameters for phase identification were usually from 10-70 º2θ with 0.04 º2θ/step and 3 sec/step, with longer scans of 0.02 º2θ/step and 8 sec/step for samples used for lattice parameter calculation. Samples were mixed with LiF as an internal calibration standard. The cell volume was calculated using a least-squares method.[2]

2.3 Results and Discussion

Table 2-I summarizes the X-ray phase analysis of the samples prepared in this study. The samples contained different phases including β-gallia, corundum, rutile, pseudobrookite and various intergrowths with $n \geq 15$. X-ray diffraction patterns for the Ga_2O_3-Al_2O_3 system (n = 4) are given as Figure 2.2. Samples prepared with $x < 0.6$ contained only a beta-gallia phase. Those prepared with $x \geq 0.9$ contained corundum. The sample prepared with x = 0.8 was biphasic. For the single phase samples, the peak shift toward higher angles with increasing Al_2O_3 content is indicative of decreasing cell volume, confirmed by lattice parameter calculations, which are given in Figure 2.3. The substitution of smaller Al^{3+} ions for Ga^{3+}ions (for CN = 4, Al^{3+}:0.39Å vs. Ga^{3+}: 0.47Å [13]) decreases the size of the lattice. The solubility limits were determined by assuming that the unit cell volume vs. composition relationships were linear in the single phase regions and that the unit cell volume did not increase once the solubility limit had been exceeded. The solubility limit of Al^{3+} in the β-gallia structure determined in this manner (78%) was intermediate between that reported by Hill and Roy[8] (67 mole %) and Mizuno et al.[9] (85 mole %). However, note that the data points are not linear, where they are expected to be

[2] Jade, XRD Analysis Software from Materials Data Inc. (1998)

linear. As illustrated in Figure 2.3, the solubility of Ga^{3+} into corundum is ~12%. The data from this study show a lower solubility of Ga^{3+} into corundum than reported by Hill and Roy[8] (30 %), but is in good agreement with that reported by Mizuno et al.[9] (15%).

Table 2-I. Summary of Results for the Stoichiometry, $Ga_{4-4x}Al_{4x}Ti_{n-4}O_{2n-2}$.[3]

		x													
		0	0.1	0.2	0.3	0.4	0.5	0.6	0.7	0.75	0.8	0.85	0.9	0.95	1.0
n-value	4	BG	-	BG	-	BG	-	BG	-	-	BG, C	-	C	C	C
	5	-	PB, BG	-	PB, BG	-	PB, BG	-	PB, BG	PB,BG	PB, BG, C	PB, C	PB, C	-	-
	6	PB	PB	-	PB	-	PB	-	PB	-	-	-	PB	-	PB
	7	-	PB, I	-	PB, I×2	-	PB, I	-	-	-	-	-	-	-	-
	9	PB, I	PB, I	-	PB, I×2	-	PB, I	-	-	-	-	-	PB, R	-	-
	15	I	I, PB	-	I×2, PB	-	I, PB	-	-	-	-	-	-	-	-
	17	I	I	-	I×2, PB	-	-	-	-	-	-	-	-	-	-
	19	I	-	-	-	-	-	-	-	-	-	-	-	-	-
	21	I	-	-	I×2, PB	-	-	-	-	-	-	-	-	-	-
	23	I	-	-	-	-	-	-	-	-	-	-	-	-	-
	25	I	I	I	I×2, PB	-	I, PB, R	-	PB, R	-	-	-	-	-	-
	27	I	I	-	-	-	-	-	-	-	-	-	-	-	-
	29	-	-	I	-	-	-	-	-	-	-	-	-	-	-

[3] BG: β-gallia solid solution, C: corundum solid solution, PB: pseudobrookite solid solution, I: intergrowth, I×2: two intergrowth phases, R: rutile (TiO_2), (-) indicates composition not tested.

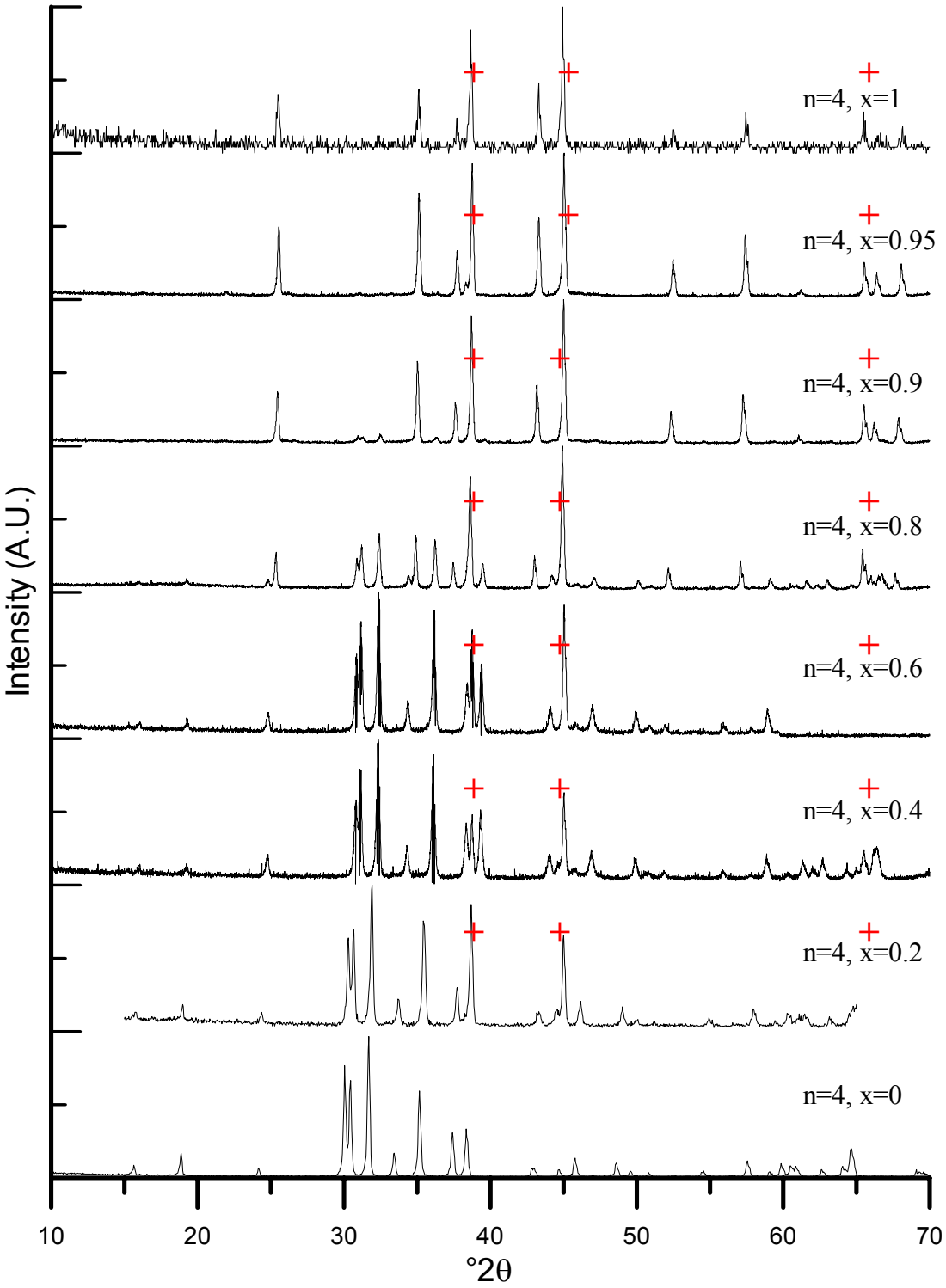

Figure 2.2. X-ray diffraction patterns of samples prepared as n = 4 according to $Ga_{4-4x}Al_{4x}Ti_{n-4}O_{2n-2}$. (+) indicates peaks for the LiF standard.

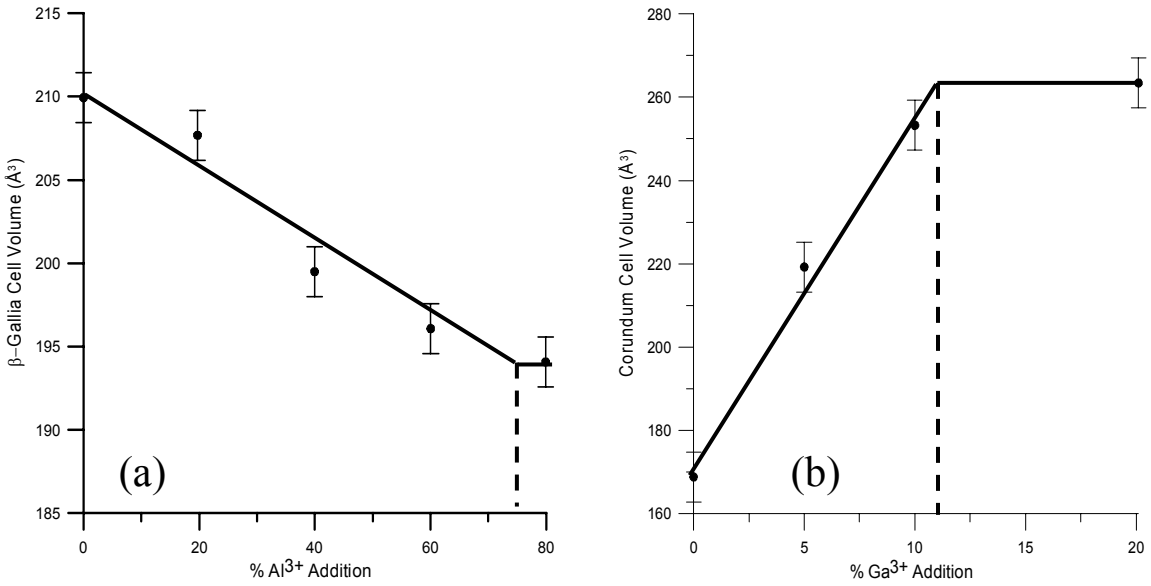

Figure 2.3. Lattice volume as a function of concentration for (a) β-gallia and (b) corundum solid solutions. Straight lines were added as a guided eye fit.

Figure 2.4 shows the x-ray diffraction patterns of samples prepared as n = 6, $0 \leq x \leq 1.0$. A continuous solid solution between Ga_2TiO_5 and Al_2TiO_5 was observed. A decrease in lattice size with increasing Al^{3+} cations was expected, and confirmed by peaks shifting right and by the calculated lattice parameters shown in Figure 2.5.

Samples prepared as n = 15-25 (where n is odd only, (x = 0), n = 17, 25, 27 (x = 0.1) and n = 25, 29, (x = 0.2) were judged to be phase-pure intergrowths. However, the x-ray diffraction patterns of intergrowth phases are generally similar, as shown in Figure 2.6 often making it difficult to distinguish between different intergrowths.

The remaining samples were multiphase. Samples prepared as n = 5, $0.1 \leq x \leq 0.75$ contained the β-gallia solid-solution and the pseudo-brookite solid-solution, and those prepared as n = 5, $0.85 \leq x \leq 1.0$ contained corundum solid-solution and pseudobrookite solid-solution. The n = 5, x = 0.8 sample was triphasic.

Samples prepared as n = 7 and 9, x = 0.1 and 0.3 contained intergrowth and pseudo-brookite solid solution, while the sample prepared as n = 9, x = 0.9 contained rutile and pseudo-brookite solid solution. The sample prepared as n = 25, x = 0.5 was triphasic with rutile, pseudobrookite and n = 33 intergrowth. The samples prepared as n = 7, 9, 15, 17, 21 and 25, x = 0.3 were triphasic with rutile, along with n = 21 and n = 33 intergrowths.

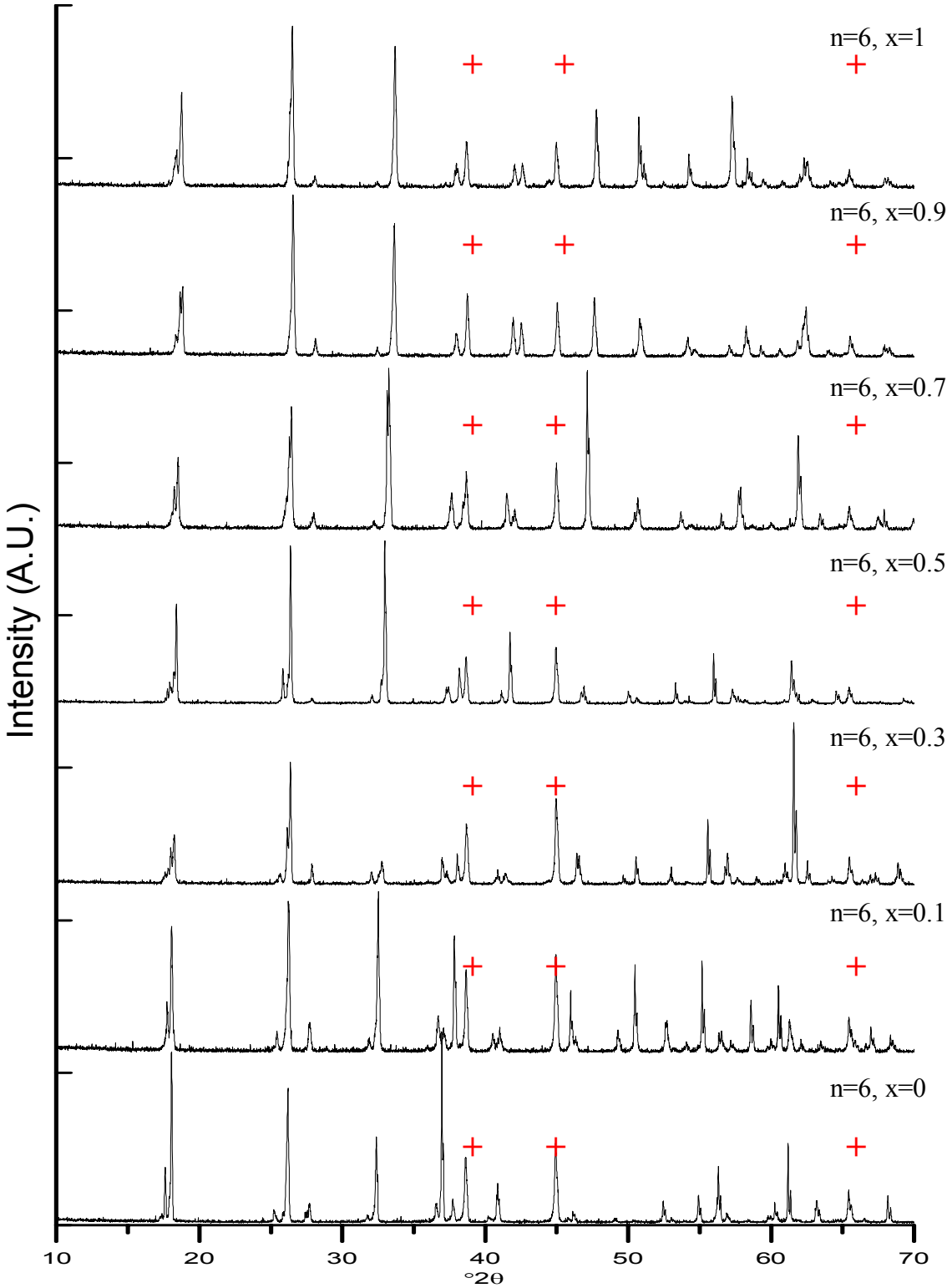

Figure 2.4. X-ray diffraction patterns for samples prepared as n = 6 according to $Ga_{4-4x}Al_{4x}Ti_{n-4}O_{2n-2}$. The (+) symbol indicates peaks from the LiF standard.

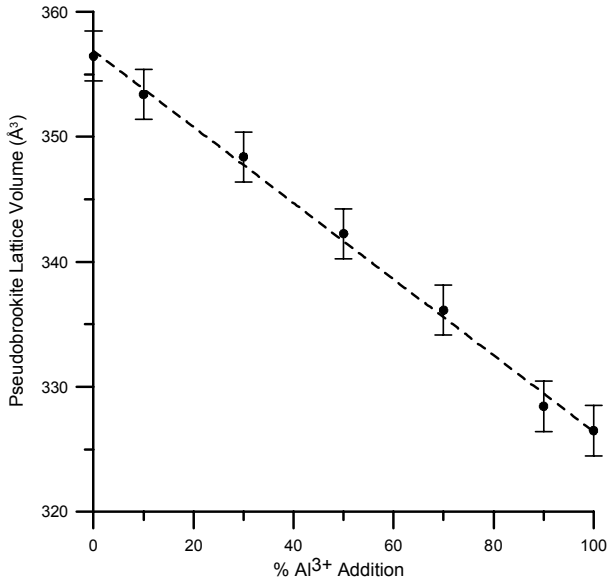

Figure 2.5. Lattice volume as a function concentration for pseudobrookite solid solution, with a linear fit.

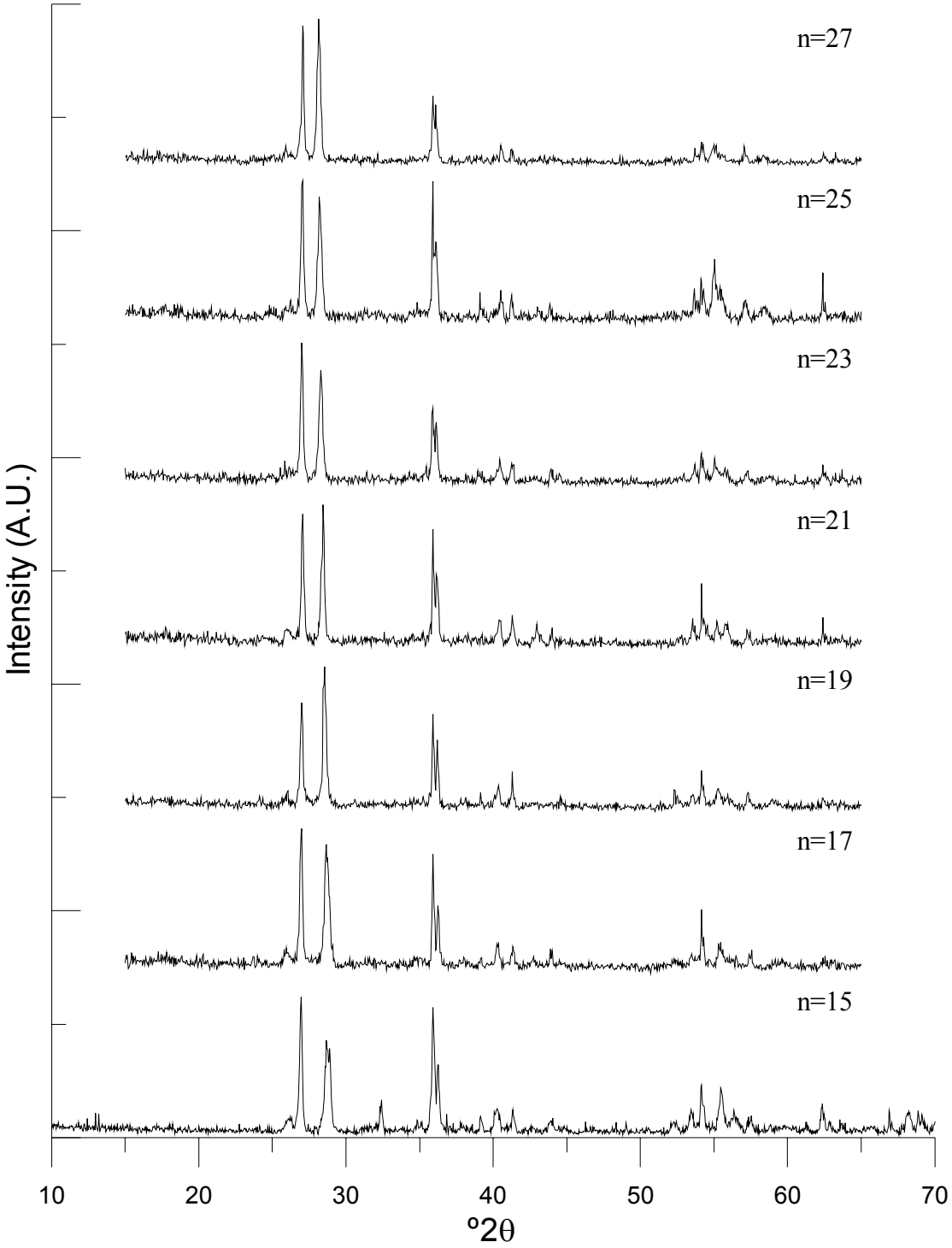

Figure 2.6. XRD data of intergrowth phases with no alumina substitution.

The phase analyses were used to construct a sub-solidus phase diagram for the Ga_2O_3-Al_2O_3-TiO_2 system (Figure 2.7). Solid circles indicate phase pure samples, open

circles indicate biphasic samples and triangles indicate triphasic samples. Solid solutions are shown as thick horizontal lines, where tie lines are shown as dashed lines.

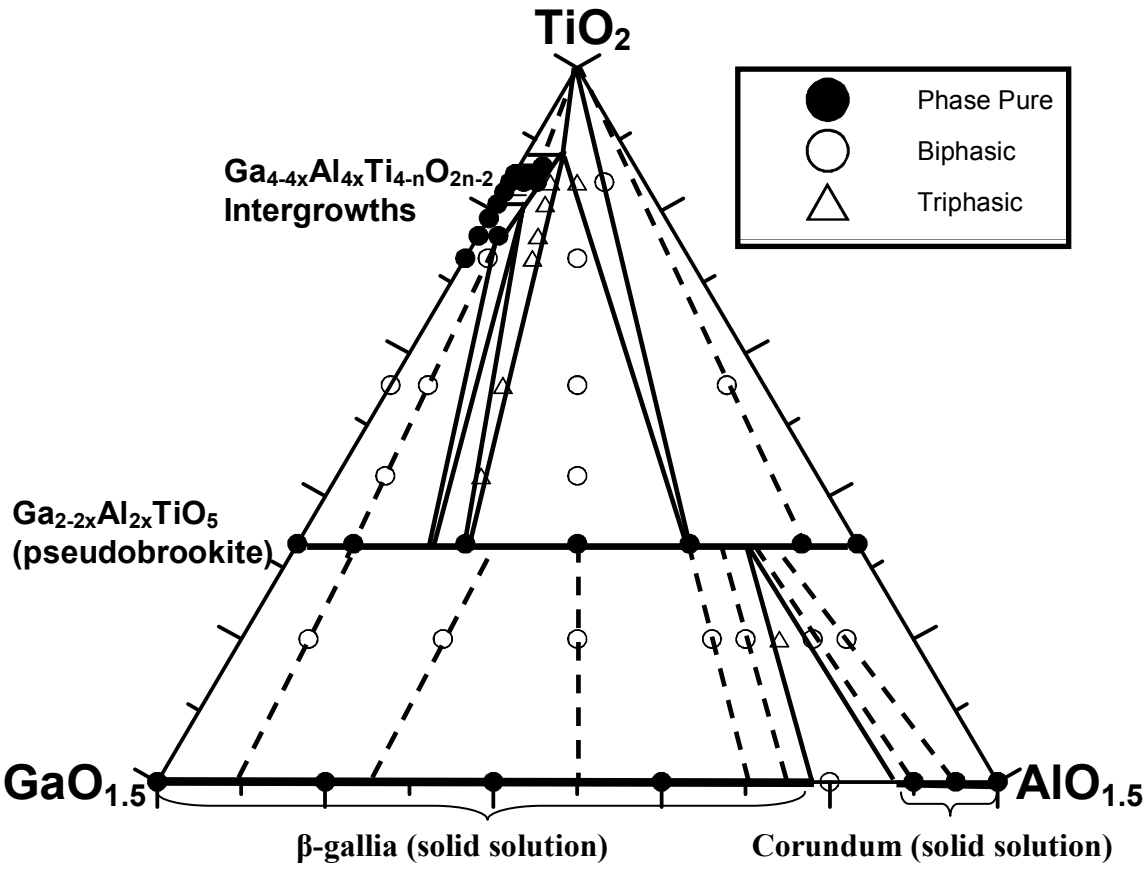

Figure 2.7. Proposed sub-solidous phase diagram at 1400ºC.

As mentioned previously, there is a pseudobrookite solid solution, and the solubility ranges for the beta-gallia and corundum phases were determined from lattice parameter measurements. Where possible, tie lines were drawn by comparing the lattice parameters of phases in the biphasic mixtures to the lattice parameters of the phase-pure beta-gallia, corundum and pseudobrookite solid solutions. In situations where this was not possible, the solubility limit was estimated from the position of a single diffraction peak. The (230) peak at 32-33.5º2θ was used for pseudobrookite and the (111) peak at 35-36.5 º2θ was used for beta-gallia. Samples containing rutile show no peak shift in the

rutile peaks, as expected, because neither gallium nor aluminum is able to take on the 4^+ oxidation state required to enter the rutile structure.

Because the x-ray diffraction patterns of intergrowth phases are generally similar (Figure 2.6), it was often difficult to identify the n values of intergrowths in multiphase samples. However, an inverse relationship between the separation of two prominent peaks (~27º2θ (-8 0 3) and ~28.5º2θ (14 0 1) in the diffraction patterns of phase-pure, x = 0 intergrowths and the corresponding n value was recognized, as shown in Figure 2.8 and Figure 2.9. This correlation was used to identify the approximate n value of the intergrowths in multiphase samples. In general, most of the multi-phase samples contained n = 17, n = 21, and n = 33 intergrowths. The analysis of the biphasic and triphasic samples was used to infer the approximate solid solution ranges for these intergrowth phases, which in general was $x < \sim 0.25$ Because the other intergrowth phases were not noted in the multiphase samples, they are assumed to have somewhat smaller solubility ranges. Clearly, there is a considerable amount of uncertainty with regards to the solubility limits of the intergrowths and their phase relationships with each other.

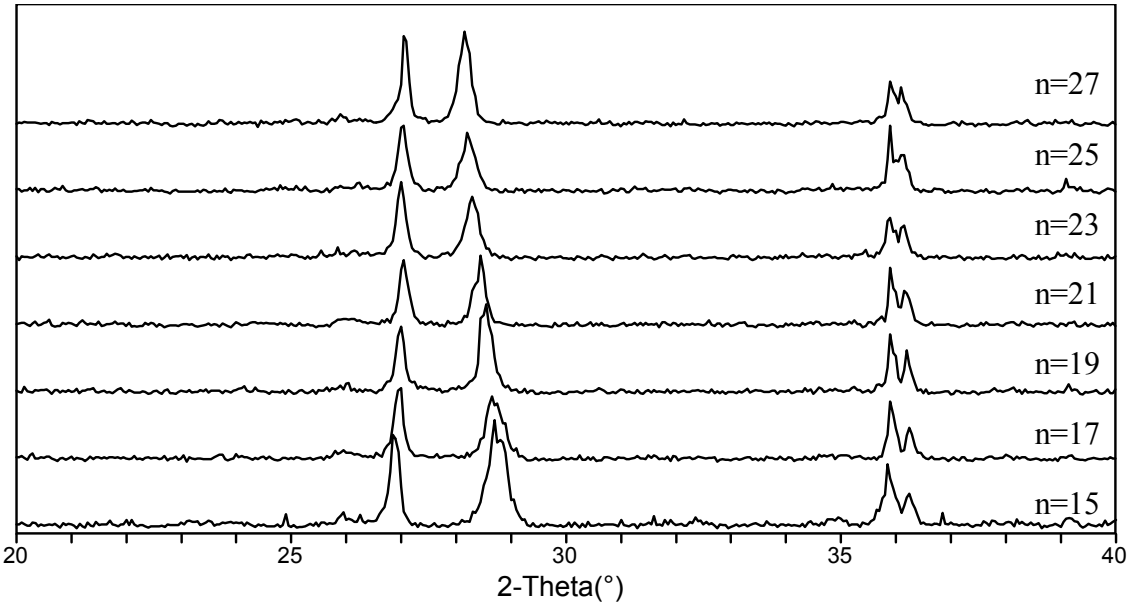

Figure 2.8. X-ray diffraction patterns for intergrowth samples with x=0, showing decrease in peak spacing with increasing n-value.

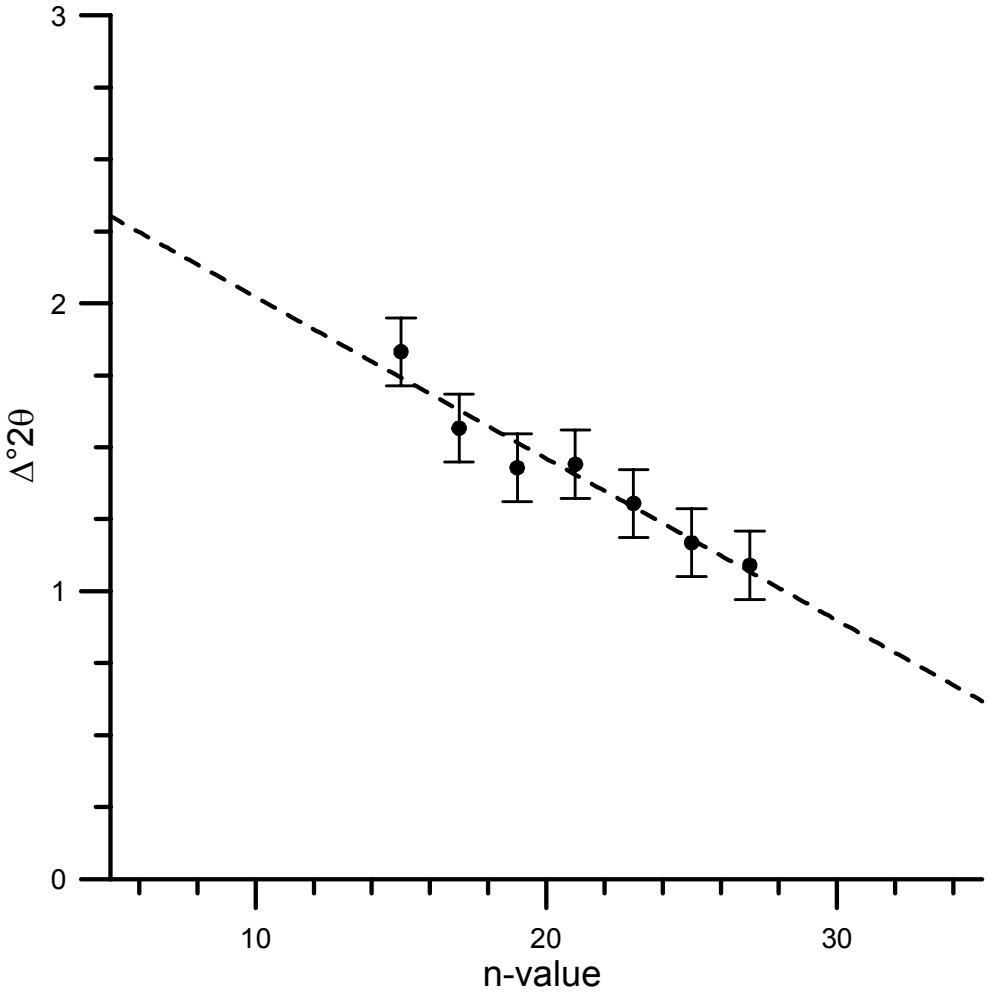

Figure 2.9. Graph of Δº2θ versus n-value for x = 0 intergrowths, where Δº2θ refers to the distance between two diffraction peaks, (-8 0 3) and (14 0 1) in the intergrowth diffraction pattern. This graph was used to approximate the composition of unknown intergrowth phases.

2.4 Conclusions

The substitution of aluminum for gallium does not stabilize $n \leq 15$ intergrowths at 1400ºC. Thus, the Ga_2O_3-Al_2O_3-TiO_2 system does not appear to be a good candidate for ion storage applications.

In addition to high-n intergrowths, the Ga_2O_3-Al_2O_3-TiO_2 system forms beta-gallia, pseudobrookite, and alumina solid solutions. The substitution of Al^{3+} for Ga^{3+} reduces the cell volume of the β-gallia and pseudobrookite structures. The substitution of Ga^{3+} for Al^{3+} increases the cell volume of corundum.

2.5 References

1. A. Kahn, V. Agafonov, D. Michel, and M.P.Y. Jorba, "New Gallium Germanates with Tunnel Structures: α-Ga_4GeO_8 and $Ga_4Ge_3O_{12}$," *J. Solid State Chem.,* **65** [3] 377-82 (1986).

2. M.B. Varfolomeev, A.S. Mironova, T.I.Dudina, and N.D. Koldashov, "Interaction of Gallium (III) Oxide," *Zh. Neorg. Khim.,* **20** [6] 3140-41 (1975).

3. A.M. Lejus, D. Goldberg, and A. Revcolevschi, "New Compounds Formed from Rutile, TiO_2 and Oxides of Trivalent and Quadrivalent Metals," *C. R. Seances Acad. Sci., Ser. C,* **263** [20] 1223-26 (1966).

4. R.M. Gibb and J.S. Anderson, "Electron Microscopy of Solid Solutions and Crystallographic Shear Structures," *J. Solid State Chem.,* **5** [1] 212-25 (1971).

5. D.J. Lloyd, I.E. Grey, and L.A. Bursill, "The Structure of $Ga_4Ti_{21}O_{48}$," *Acta. Crystallogr.,* **32B** [11] 1756-61 (1975).

6. S. Kamiya and R.J.D. Tilley, "Phase Relations in the Pseudobinary System TiO_2-Ga_2O_3," *J. Solid State Chem.,* **22** [1] 205-16 (1977).

7. L.A. Bursill and G.G. Stone, "Tunnel and Intergrowth Structures in the Gallia-rich Gallium Titanate System," *J. Solid State Chem.,* **38** [1] 149-57 (1981).

8. V.G. Hill, R. Roy, and E.F. Osborn, "The System Alumina-Gallia-Water," *J. Am. Ceram. Soc.,* **35** [6] 135-42 (1952).

9. M. Mizuno, T. Yamada, and T. Noguchi, "The Liquidous Curve in the System Al_2O_3-Ga_2O_3 as Measured with a Solar Furnace," *Dainippon Yogyo Kyokai Zasshi,* **83** [4] 175-7 (1975).

10. H. Muller-Bushbaum, "Zur Kristallchemie von Ga_2TiO_5," *Z. Naturforsch.,* **29b** 590-3 (1974).

11. S.M. Lang, C.L. Fillmore, and L.H. Maxwell, "The System Beryllia-Alumina-Titania: Phase Relations and General Physical Properties of Three-Component Porcelains," *J. Res. Natl. Bur. Stand.,* **48** [4] 298-312 (1952).

12. B.N. Bhattacharyya and S. Sen, "Aluminium Titanate," *Cent. Glass Ceram. Res. Inst. Bull.,* **10** [4] 115-23 (1963).

13. R.D. Shannon, "Revised Effective Ionic Radii and Systematic Studies of Interatomic Distances in Halides and Chalcogenides," *Acta Crystallogr.,* **A32** [3] 751-67 (1974).

3 Processing and Analysis of Gallium-Manganese Oxides

3.1 Introduction

The goal of this study was to prepare β-gallia rutile intergrowth structures using MnO_2 as the rutile-structured component with the stoichiometries, $Ga_4Mn_{n-4}O_{2n-2}$. The oxides of manganese have been widely researched as materials for ion-storage. In general, manganese oxides are attractive materials because of the large number of oxidation states manganese is able to take on (2^+, 3^+, 4^+ and 7^+) and for the consequent large number of structure types.[1]

In this study, the oxidation state of interest is Mn^{4+}. Figure 3.1 shows the equilibrium dissociation pressures of oxygen from Klingsberg and Roy.[2] The dashed line represents the extrapolation of the MnO_2 to Mn_2O_3 transition where the equilibrium temperature at 1 atm is about 250°C. Therefore, it is necessary to use low temperatures in order to retain MnO_2 as is required for β-gallia rutile intergrowths. For this reason, hydrothermal synthesis was used in this work.

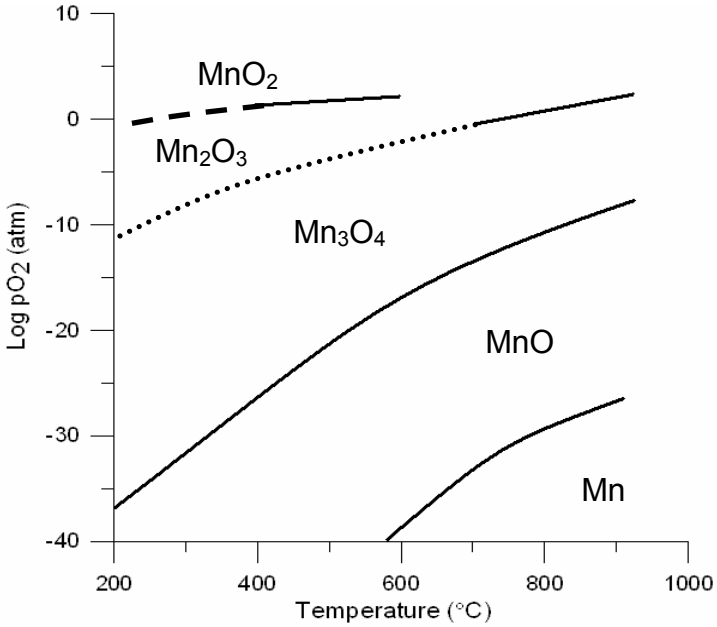

Figure 3.1. Equilibrium dissociation pressures of oxygen from Klingsberg and Roy,[2] with data from Coughlin[3] and Tatievskaya.[4] The dashed line is an extrapolation showing dissociation at 250ºC and 1 atm reported by Klingsberg and Roy and dotted line is extrapolation of the average of data on the Mn_2O_3 to Mn_3O_4 transition.

Hydrothermal synthesis has been of recent interest for use in processing inorganic materials. This process originates from the interest in artificially preparing minerals, by mimicking the high pressures and temperatures attained in nature.[5] It involves the heating of reactants as a solution or suspension at high temperature and pressure. The solvent is generally water, with temperatures between the boiling point and the critical temperature, which is about 374ºC for water. Pressures are normally up to 20MPa. A benefit of hydrothermal synthesis is the ability to attain small particles with a narrow size distribution with high purity and good chemical homogeneity, at much lower temperatures and heating times than traditional solid state synthesis.[6] As opposed to other innovative processing methods, hydrothermal synthesis does not require high-temperature calcinations such as with sol-gel and Pechini processes,[7] and there is no need for grinding, which can add impurities and time. Also, hydrothermal conditions often result in structures not producible under any other method.[5,8]

Maintaining control of the processing parameters in hydrothermal synthesis is extremely difficult. If not successful, different products can result from seemingly the same conditions, and are therefore difficult to reproduce.[9] Processing parameters can include but are not limited to, pressure, which is related to the amount of liquid and its vapor pressure, pH, temperature, heating rate, heating time and starting material composition.[8]

A summary of all relevant structures and transitions in the Mn-O-H system is given in Table 3-I. Of all the manganese oxide structures, γ-MnO_2 (Nsutite) is the most frequently used by the battery industry. It is the primary structure in aqueous Zn/MnO_2 and Li/MnO_2 cells. Its structure is an intergrowth between β-MnO_2 (pyrolusite, which has the rutile structure), and ramsdellite-MnO_2, both of which are orthorhombic. These structures are given as Figure 3.2. This intergrowth between β-MnO_2 and ramsdellite-MnO_2 produces 2x1 tunnels available for lithium insertion. Improved electrochemical cycling can be achieved through pre-lithiation, meaning lithium is inserted during the processing step. The spinel $LiMn_2O_4$[1,7] has lithium already incorporated and is currently the most widely studied manganese battery material. There is also recent interest in manganese oxides with semi-amorphous structures for battery applications.[10]

Other manganese structures of interest to this study are hausmannite, spinel-structure, bixbyite and the oxyhydroxides. There are two types of manganese oxide referred to as Hausmannite. Alpha-Mn_3O_4 is tetragonal. Beta-Mn_3O_4 is cubic with a spinel structure. There are two types of bixbyite also: α-Mn_2O_3 is cubic and β-Mn_2O_3 is orthorhombic. There are two octahedrally coordinated Mn^{3+} oxyhydroxides. Isostructural with α-AlOOH and α-GaOOH, α-MnOOH (groutite) is orthorhombic and has a diaspore type structure. Gamma-MnOOH is monoclinic (manganite) and is structurally related to β-MnO_2. The structure of β-MnOOH (Feitknechtite) is not well-characterized but is known to be tetragonal.[11]

Upon heating these phases, a number of transitions can occur, including dehydroxylation, reduction or even oxidation. These transitions and temperatures are dependent upon processing conditions and whether the compound is stable or metastable. In general, heating manganese oxyhydroxide will result in dehydroxylation and then a series of reductions as follows:

$$\alpha\text{-MnOOH} \xrightarrow{300\,^{\circ}C} \beta\text{-}MnO_2 \xrightarrow{640^{\circ}-800\,^{\circ}C} \beta\text{-}Mn_2O_3 \xrightarrow{900\,^{\circ}C} \beta\text{-}Mn_3O_4$$

Gallium is typically trivalent. Only β-Ga_2O_3 is stable,[12] but up to four polymorphs of Ga_2O_3 exist. All of the known gallium oxides transform to β-gallia upon heating, as summarized in Table 3-II. These polymorphs are α-Ga_2O_3, which is hexagonal and isostructural to α-Al_2O_3; β-Ga_2O_3 which is monoclinic and isostructural with θ-Al_2O_3;[13] γ-Ga_2O_3, which is a distorted cubic-defective spinel isostructural with γ-Al_2O_3; and δ-Ga_2O_3 which is cubic and isostructural with α-Mn_2O_3 (bixbyite).[12,14] The oxyhydroxide, α-GaOOH, is isostructural with α-AlOOH (diaspore) and α-MnOOH (groutite).[15] A typical reaction sequence for the heating of α-GaOOH is:[16,17]

$$\alpha\text{-GaOOH} \xrightarrow{500\,^{\circ}C} \alpha\text{-}Ga_2O_3 \xrightarrow{500^{\circ}-750\,^{\circ}C} \beta\text{-}Ga_2O_3$$

Table 3-I. Manganese Oxides and Oxyhydroxidesand Their Relevant Phase Transitions.

PDF #	Chemical Formula	Mineral Name	Symmetry/ Structure	Observed Phase Transitions			Ref.
				Temperature (°C)	Resultant Phase	ΔH	
07-0230	MnO	Magnetosite	Cubic	380	β-MnO_2	+	18
12-0733	α-MnOOH	Groutite	Orthorhombic/ Diaspore	300	β-MnO_2	+	15,19
18-0804	β-MnOOH	Feitknechtite	Tetragonal				11
74-1842	γ-MnOOH	Manganite	Monoclinic	300-400 380	β-MnO_2 $MnO{\cdot}MnO_2$	+	18-20
24-0735	β-MnO_2	Pyrolusite	Tetragonal/ rutile	640-800	Mn_2O_3	+	18,20,21
39-0375	MnO_2	Ramsdellite	Orthorhombic/ Diaspore	0-500 600	β-MnO_2 Mn_2O_3	+	22
17-0510	γ-MnO_2	Nsutite	Hexagonal	300-400	β-MnO_2	?	23
41-1442	α-Mn_2O_3	c-Bixbyite	Cubic	35	β-Mn_2O_3	+	24
24-0508	β-Mn_2O_3	o-Bixbyite	Orthorhombic	960	β-Mn_3O_4	+	18,21
24-0734	α-Mn_3O_4	α-Hausmannite	Tetragonal	1130-1170	β-Mn_3O_4	+	25-27
04-0732 13-0162	β-Mn_3O_4	β-Hausmannite	Cubic/Spinel	Stable above 960			28

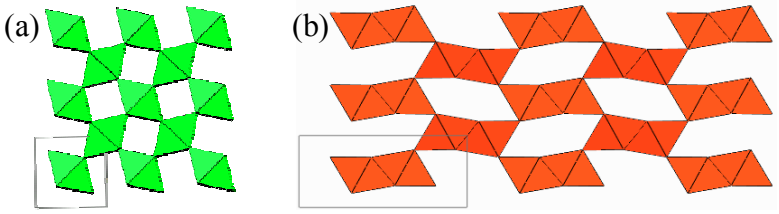

Figure 3.2. Crystal structures of (a) pyrolusite (rutile-structure) and (b) ramsdellite, where γ-MnO_2 is an intergrowth of these structures, forming 1×2 tunnels.

Table 3-II. Gallium Oxides and Oxyhydroxides and Their Relevant Phase Transitions.

PDF#	Composition	Crystal System/ Structure	Transition			Ref
			Temperature (°C)[4]	Resulting Phase	ΔH	
73-1028 06-0180	α-GaOOH	Orthorhombic/ Diaspore	500(D)	α-Ga_2O_3	+	12,17
18-0532	$Ga(OH)_3$	Cubic			?	29
06-0503	α-Ga_2O_3	Hexagonal	300(W) 600(D)	β-Ga_2O_3	+	12,17
20-0426	δ-Ga_2O_3	Cubic	300(W)	β-Ga_2O_3	+	12
76-0573	β-Ga_2O_3	Monoclinic		Stable		30

Only recently has a study been conducted on the Ga_2O_3-MnO_2 system which was done by Escribano et al.[14] A coprecipitation method was used where samples were aged at low temperatures under continuous stirring with pH of about 8. Samples were prepared with varying z-values according to $Mn_zGa_{1-z}O_y$, of which z = 0.5 and z = 0.2 are of particular interest to this study. The resultant samples were heated and analyzed using x-ray diffraction, IR and UV-visible-NIR spectroscopies. The following transition/reaction sequences were reported:

$$z = 0.2: \text{ diaspore} \xrightarrow{450\,^\circ C} \delta\text{-gallia} \xrightarrow{600\,^\circ C} \beta\text{-gallia} \xrightarrow{800\,^\circ C} \text{orthorhombic-bixbyite}$$

$$z = 0.5: \text{ diaspore} \xrightarrow{450\,^\circ C} \delta\text{-gallia} + \text{hausmannite} \xrightarrow{600\,^\circ C} \beta\text{-gallia} + \text{hausmannite} \xrightarrow{800\,^\circ C} \beta\text{- gallia} + \text{spinel}$$

Escribano et al.[14] concluded that many of the known Ga- and Mn-oxide and oxyhydroxide phases have a reciprocal solubility.

The Ga_2MnO_4 phase is the only known oxide compound of manganese and gallium. It has a cubic spinel crystal structure and is said to be stable from 960ºC to its melting temperature.[31] In the spinel structure, both trivalent and divalent manganese can be present, i.e. $(Ga_{2-x}Mn_x)^{3+}Mn^{2+}O_4$.

In this study, compositions were prepared as $Ga_4Mn_{n-4}O_{2n-2}$, where n = 5, 7, and 9, using hydrothermal synthesis. Samples were prepared with pH ranging from 0.7 to 9.8,

[4] (D) indicates temperature is for dry processing, and (W) indicates transformation in aqueous conditions.

and temperature ranging from 150º to 235ºC, and autogenic pressure. The resulting powders were characterized using x-ray diffraction, thermal gravimetric analysis and differential scanning calorimetry. In addition to known oxides and oxyhydroxides, several unidentified phases were observed.

3.2 Experimental

Samples were prepared using a conventional hydrothermal process in a 23mL Parr vessel with a Teflon sample cup. The starting materials, $Ga(NO_3)_3 \cdot xH_2O$ (powder) and $Mn(NO_3)_2$ (aq.), were analyzed using inductively coupled plasma (ICP) and thermal gravimetric analysis (TGA) to determine exact water content. Samples were weighed to yield 1 gr of final oxide. The pH was adjusted in the range of 0.7 to 9.8 using NH_4OH and/or HNO_3 and was measured using an AR20 pH meter (Acumet), with the final water content about 15mL. Samples were placed in a cold furnace and heated to final temperature and were allowed to cool in the furnace after heating was complete. Temperatures ranged from 150º to 230ºC, heating times ranged from 18 to 104 hours and calculated pressures ranged from 1000 to 1800 psi. The samples were then filtered using a Büchner funnel and vacuum, and then heated overnight in a 60ºC drying oven.

Additional samples were synthesized using microwave hydrothermal synthesis. A laboratory microwave unit (UDV-10, CEM) was used with 100mL Teflon sample cups with a final sample size of 5 grams. The pressure and temperature ranged from 100 to 200 psi and 200ºC. Heating time was 15-20 minutes.

Samples were characterized by x-ray diffraction (XRD) on a Phillips XRG3100 diffractometer using Cu Kα radiation (40kV, 20mA). Scans were conducted from 10-70º2θ with a step rate of 0.04º/step and 3 sec/step. Some samples were mixed with LiF as an internal calibration standard. The lattice parameters were calculated using a least-squares method.[5] For phase analysis, all samples were compared to the powder diffraction files (PDFs) given in Table 3-III.

[5] Jade, XRD Analysis Software (1998).

Energy minimization calculations were conducted using the General Utility Lattice Program (GULP)[6] on β-gallia rutile intergrowth structures with compositions n = 5, 6, 7 and 9 to estimate atom positions and lattice parameters for the desired phases. These atom positions and lattice parameters were then used to generate x-ray diffraction patterns (Cu-Kα radiation) using PowderCell,[7] for comparison to unidentified phases. The calculated X-ray diffraction patterns are given in Figure 3.3.

Table 3-III. Powder Diffraction File Entries Used to Determine Sample Composition.

Composition	Powder Diffraction File Entry Numbers
Ga_2O_3	06-0609, 20-0426, 06-0529, 06-0503, 76-0573
GaOOH	73-1028, 06-0180, 26-0674
$Ga(OH)_3$	18-0532
$Mn(OH)_2$	73-1133, 18-0787
MnO	78-0424, 07-0230
Mn_3O_4	04-0732, 80-0382, 18-0803, 86-2337, 24-0734, 86-2337,13-0162
Mn_2O_3	24-0508, 41-1442, 33-0900
MnO_2	72-1982, 50-0866, 44-0141, 72-1984, 30-0820, 72-1983, 24-0735
Mn_5O_8	39-1218
$Mn(OH)_4$	15-0604
MnOOH	18-0804, 12-0733, 41-1379, 74-1842, 81-1946, 75-1199
Ga_2MnO_4	36-0181, 72-1521

[6] General Utility Lattice Program, Energy Minimization Program (1998).
[7] PowderCell, XRD Pattern Generation Program and Structure Generation, (2000).

In order to get insight as to the composition of the unidentified phases, thermal analysis was conducted. TGA was used to determine weight loss and transition temperatures for comparison to calculated and published values. Differential scanning calorimetry (DSC) was used to determine the differential heat gradient between an empty reference pan and the sample. Endothermic reactions can be a transition from a phase stable at low temperatures to a phase stable at high temperatures, a loss of volatile components such as H_2O or CO_2, or a reduction in the oxidation number, such as from M^{4+} to M^{3+}. Exothermic reactions are the opposite transitions.[32] Transition temperatures different from published values were to be expected, with the addition of dopants and different processing conditions.[9,12]

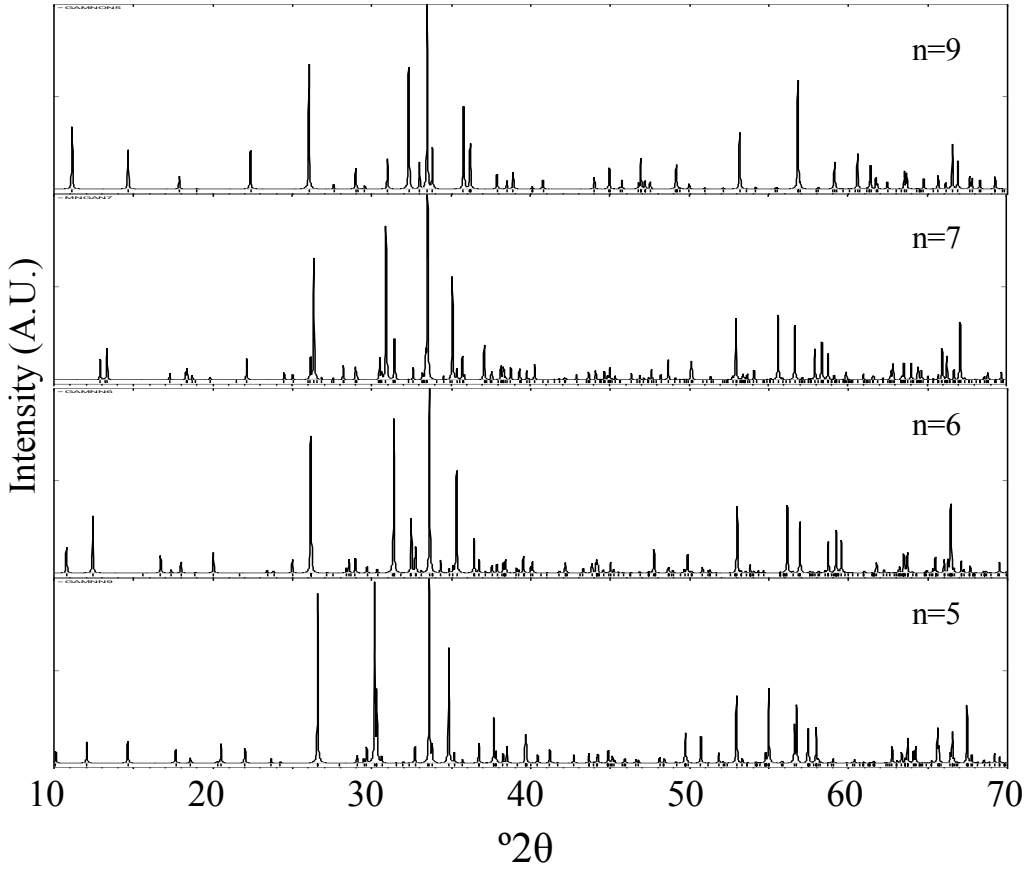

Figure 3.3. Calculated diffraction patterns (Cu Kα radiation) for hypothetical Mn-containing intergrowth phases. Phases n = 5 and n = 9 were calculated assuming a symmetry of C2/m, while phases n = 6 and n = 7 were calculated assuming a symmetry P2/m.[33]

A DSC Q10 (TA Instruments) was used. A baseline was measured with an empty sample pan and then subtracted from the sample measurement, both with the parameters of 10ºC/min to 725ºC. TGA was conducted using a TGA Q50 (TA Instruments) with a heating rate and final temperature of 20ºC/min and 1000ºC, respectively. Both analyses used platinum pans and nitrogen as the purge gas.

Using the DSC/TGA data as a guide, fresh samples containing unidentified major phases were heated to selected temperatures and analyzed using x-ray diffraction to track phase evolution upon heating.

3.3 Results and Discussion

3.3.1 Nomenclature

In this study, several unidentified phases were observed in x-ray diffraction patterns. The unidentified phases occurred either as a major phase or as a minor phase in association with known phases. For convenience, abbreviations will be used to describe unidentified phases and peaks.

Minor phase unidentified phases are phases with unidentified peaks occurring with relative intensities < 5%, in addition to determinable major phases. These minor unidentified peaks were generally grouped according to their occurrence in relation to each other, though it is possible that each group could contain more than one phase. These minor unidentified phases will be designated with a number, where UG#1 has unidentified peaks with º2θ: 21, 33 and 36, UG#2 has unidentified peaks with º2θ: 44, usually 51, 53, and 65 and UG#3 has unidentified peaks with º2θ: 13, 19.

Unidentified major phases are those phases where no peaks could be identified with any known PDFs or hypothetical intergrowth patterns. All patterns had high background. These phases are designated with uppercase letters, such as UA, UB and UC. There is some evidence that these unidentified phases may actually contain more than one phase. To aid in the discussion of the x-ray patterns, groups of unidentified peaks are designated with by a number, UG#1, UG#2, and UG#3. Region numbers were assigned to unidentified major phase samples to help in explanation. These regions are

designated by a number, referred to as R1, R2, R3 and R4. Note these regions are different for the different unidentified major phases.

Many of the samples studied in this work are solid solutions. Because the radii of Mn^{3+} and Ga^{3+} are so similar (for CN = 6, Ga^{3+} = 0.62 Å vs. Mn^{3+} = 0.58 Å and for CN = 4, Ga^{3+} = 0.47Å vs. Mn^{3+} = 0.39 Å), it is often difficult to distinguish between the solid solution and the parent oxide using only x-ray diffraction patterns. Throughout the discussion, the solutions are identified by their corresponding mineral-group name when their structure has been positively identified. For example, the term diaspore-structure will be used generically to describe $Ga_{1-x}Mn_xOOH$ when the corresponding x-ray diffraction pattern has peaks similar to those in α-GaOOH (PDF#06-0180), where peaks could be slightly shifted.

DSC data are difficult to interpret also. Often there is no recovery to a 'zero-point' in energy transfer, so it is hard to tell whether a transition is exothermic or endothermic and any designation is usually relative to the other transitions.

3.3.2 General Results

A summary of all the processing conditions and resulting phases present is given in Table 3-IV. Graphical representations of n-value vs. pH and processing temperature vs. pH are given in Figure 3.4 and Figure 3.5, respectively. The figures summarize only the phases present after filtering and drying at 60ºC and the key given is for both figures.

The pH of the starting solution had the strongest influence on the resulting powders. Samples prepared with pH ≤ 4.2 were white whereas those prepared with pH > 4.2 were a shade of brown. Samples prepared with pH < 7 showed peaks similar to those in the diaspore α-GaOOH structure (PDF#06-0180) and with minor phase unidentified phasess. Samples with pH > 7 often contained a phase with the spinel structure (closely matching either $MnGa_2O_4$ (PDF#72-1521) or Mn_3O_4 (PDF#04-0732)), sometimes in association with a diaspore-structure phase and minor unidentified phases. Four samples with n = 9 and 9 < pH < 10 contained unidentified major phases. Color and composition were not directly related, however, since some samples with diaspore-structure were dark, therefore pH appears to be the only factor affecting color. Manganese oxides (with Mn^{2+}, Mn^{3+} and Mn^{4+}) are typically dark brown to black in color, and gallium oxides and

oxyhydroxides are typically white.[34] Therefore the origin of the color dependency is uncertain.

Table 3-IV. Summary of Processing Conditions and Results.

	Sample	n	pH	Temperature (ºC)	Time (hrs)	Phase Analysis After Drying		Phase Analysis After Heating to 1000ºC
						Major Unidentified Groups	Minor Unidentified Groups[8]	
C 1	C2S5	5	0.7	150	20	Diaspore	1,2	
C 2	C2S1	5	2.2	150	104	Diaspore	1,2	
C 3	C5S1	5	2.3	230	22	Diaspore	2	
C 4	C2S2	5	2.3	150	18	Diaspore	1,2	β-gallia
M 1	M1S1	5	2.7	200	0.25	Diaspore	2,3	
C 5	C2S6	5	4.3	150	18	Diaspore	2	
C 6	C2S3	5	6.9	150	21	Diaspore	1,2	β-gallia
M 2	M2S3	5	8.1	170	0.33	Spinel	Broad	
M 3	M2S2	5	9.0	170	0.33	Spinel	Broad	
C 7	C5S3	5	9.8	230	19	Spinel + Diaspore	1	Spinel + β-gallia
C 8	C4S1	7	3.6	150	19	Diaspore	2	
C 9	C4S2	7	8.3	150	19	Diaspore + Spinel	1,3	
M 5	M2S4	7	9.7	170	0.33	Diaspore + Spinel	Broad	
C 10	C1S5	9	0.9	150	70	Diaspore	1,2	
C 11	C6S1	9	2.1	225	18	Diaspore	1	
C 12	C5S2	9	2.1	230	19	Diaspore	1	
C 13	C1S1	9	2.1	150	65	Diaspore	1,2	
M 6	M1S2	9	2.5	200	0.25	Diaspore	2	
C 14	C1S3	9	4.2	150	2.5	Diaspore	2	
C 15	C1S4	9	4.6	150	74	Diaspore	2	
C 16	C6S3	9	6.6	225	19	Diaspore + Rutile	2	Spinel
C 17	C1S2	9	6.8	150	67	Diaspore	3	
C 18	C5S4	9	8.7	230	19	Spinel + Bixbyite	Broad	Spinel
C 19	C4S3	9	9.3	150	19	UB	1,3	Spinel + Bixbyite
M 7	M2S1	9	9.4	175	0.33	Diaspore	Broad	
C 20	C6S2	9	9.5	225	18	Spinel	Broad	
C 21	C1S6	9	9.6	150	65	UA	All UNK	Spinel + Bixbyite
C 22	C3S2	9	9.6	180	19	UC	All UNK	Spinel
C 23	C3S1	9	9.7	175	19	UA	All UNK	Spinel + Bixbyite

[8] Broad: peaks of the identified phase were broad, and therefore it was not possible to differentiate minor unidentified phases.

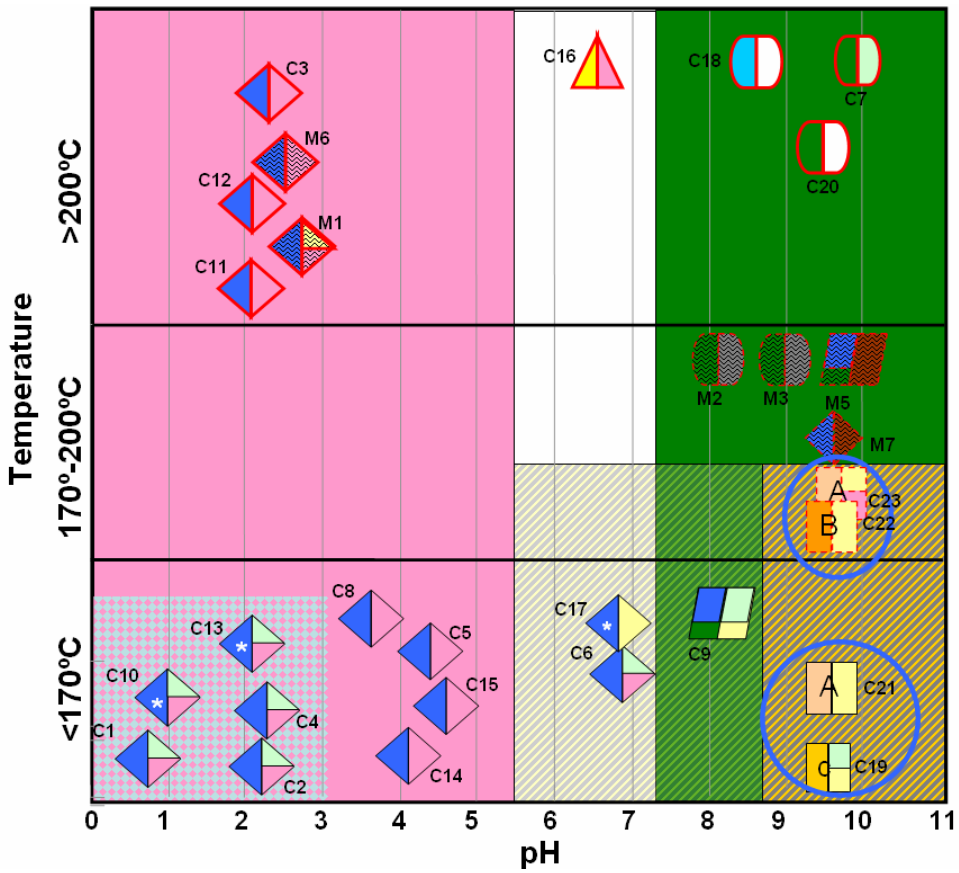

Figure 3.4. Summary of results as n-value vs. pH.

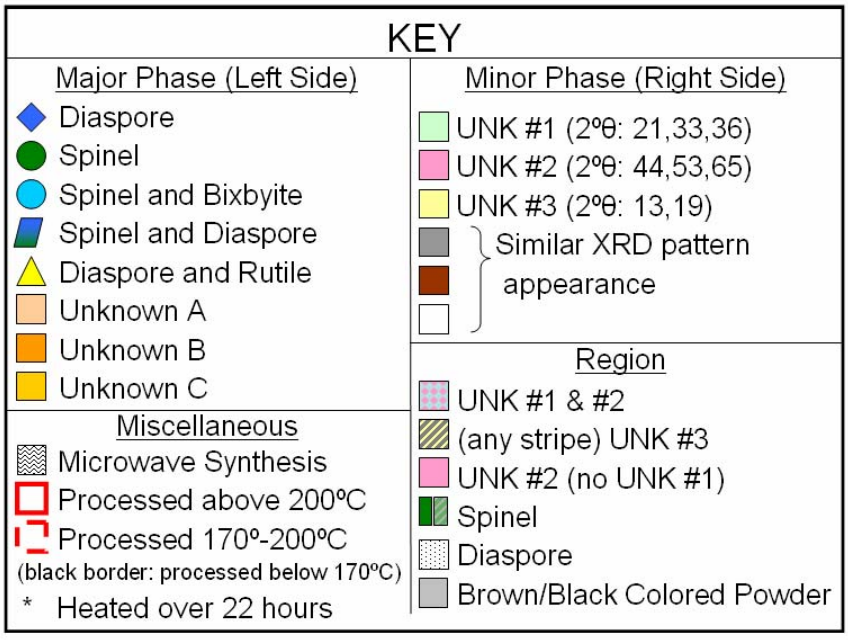

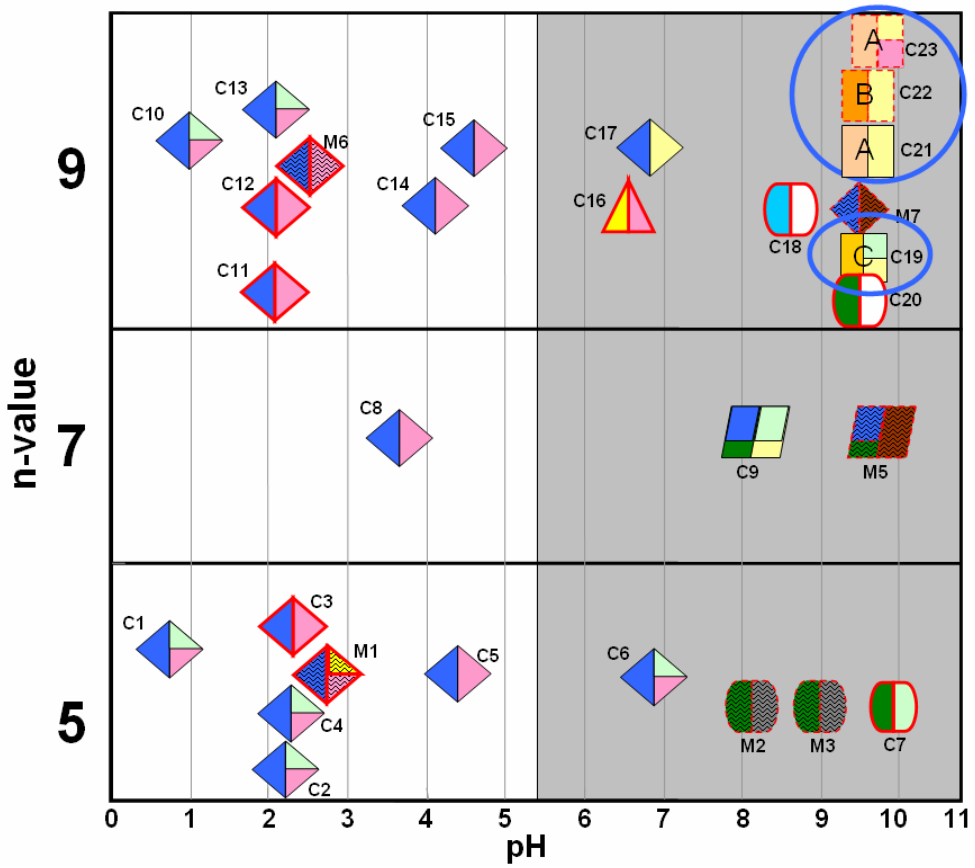

Figure 3.5. Summary of results as Temperature vs. pH.

For samples containing the diaspore-structure phase as the major phase, the occurrence of minor phase unidentified peaks gives further insight to a correlation between processing conditions and the resulting phases. For samples processed with pH < 3, those samples heated above 200ºC contained only UG#1 and do not show UG#2, whereas samples heated below 200ºC contain both UG#1 and UG#2. UG#2 may not be stable above 200ºC when prepared with this pH. UG#1 is stable at different regions, including high temperature and high pH, low temperature and high pH, and low temperature and low pH. The sample prepared with low pH via microwave hydrothermal synthesis was the only sample in this pH region to show UG#3. UG#3 was only observed in conventionally processed samples with pH > 6. It appears that microwave hydrothermal synthesis promotes the formation of UG#3 at lower pH. All samples prepared 3 < pH < 5 contained only the diaspore-structure and UG#1. Heating time and composition did not appear to have any significant affect on the products formed.

Samples prepared with 5 < pH < 8 start to show different products compared to the other pH regions. Sample C16, prepared as n = 9 with pH = 6.6 was heated to 225ºC, contains the diaspore-structure phase, the rutile-structure phase and UG#2, whereas sample C17, with similar pH heated to 150ºC, contains the diaspore-structure phase and UG#3, which was the only sample to show these two phases together. The increased heating temperature presumably discourages the formation of UG#2 in low to moderate pH samples. Also, sample C16 was the only sample of moderate pH (ranging from 3 to 8) that was heated over 200ºC. Therefore, it appears that increasing temperature is required for the formation of the rutile-structure phase. A comparison can be made between samples in the Escribano et al.[14] study and this study because the compositions are similar. For the Escribano et al.[14] study, samples prepared as z = 0.2 and z = 0.5 according to the formula $Mn_zGa_{1-z}O_y$ are similar in composition to samples prepared in this study as n = 5 and n = 9 with $Ga_4Mn_{n-4}O_{2n-2}$, respectively. More explicitly, for z = 0.2, $Mn_{0.2}Ga_{0.8}O_y$ is equal to the n = 5 composition Ga_4MnO_8 and for z = 0.5, $Mn_{0.5}Ga_{0.5}O_y$ is close to the n = 9 composition of $Ga_4Mn_5O_{16}$. They also reported the formation of β-MnO_2 in coprecipitated samples prepared as $Ga_{0.1}Mn_{0.9}O_y$ with a pH~8 at 450ºC.

Samples prepared with 8 < pH < 10 have many variations between processing conditions and results. In this region, high temperatures are most favorable for the formation of spinel-structure. Only those samples with n = 7 showed the diaspore-structure and spinel-structure, and there appears to be a correlation between microwave synthesized samples, where XRD results show broad/uncrystallized peaks of similar shape. Samples prepared in this region left uncleanable residue in the sample cup, so it is particularly possible that seeding could have affected the formation of the phases attained in this pH range. The samples with major unidentified phases, emphasized by a blue circle in Figure 3.4 and Figure 3.5, all occur in the same region with n = 9 and 9 < pH < 10. The XRD data did not match any of the powder diffraction file entries in Table 3-III or generated intergrowth patterns in Figure 3.3. This phase and other unidentified phases are not reported in the work by Escribano et al., so they may be a result of processing conditions involved with hydrothermal synthesis.

Several representative samples were selected for further analysis by DSC, TGA, TEM and XRD to gain further insight about the resulting products.

3.3.2.1 Analysis of a Diaspore-Structure-Containing Sample

Most samples with the diaspore-structure phase as the only major phase after initial processing were prepared with pH < 5 and were white. Sample C4 was selected for further analysis. This sample was prepared with n = 5, pH = 2.3, and heated to 150ºC for 18 hours. XRD showed minor unidentified phase of UG#1 and UG#2.

After heating these samples to 1000ºC, the resulting phase corresponded to the pattern for β-Ga_2O_3 (PDF#76-0573) with only minor peak shifts and x-ray patterns are given as Figure 3.6. The x-ray pattern after drying has narrow peaks, and no evidence of amorphous phases. The unidentified phases present are low intensity. It is therefore unlikely that all of the manganese present in this sample (about 20% cation) is contained within the unidentified phases; therefore, manganese must be entering the diaspore structure. However, as will be mentioned later, the change in cell volume associated with the complete dissolution of manganese into the diaspore-structure would give a lower cell volume than that seen. There is, therefore, ambiguity as to the location of the manganese.

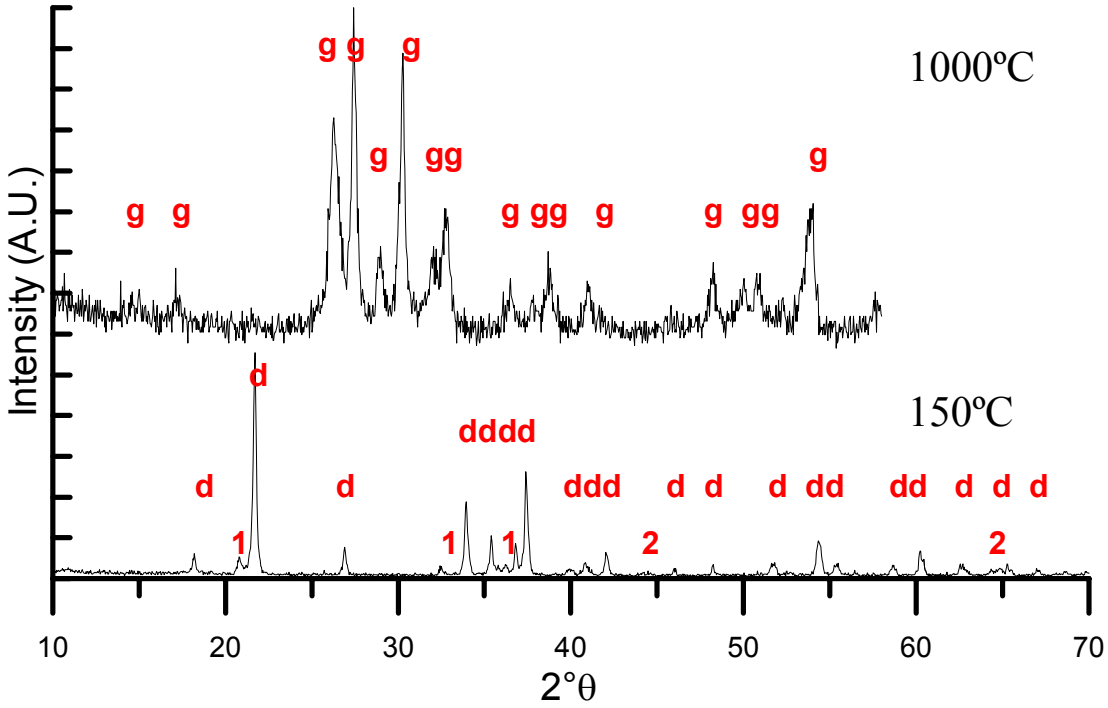

Figure 3.6. X-ray patterns of sample C4 prepared with pH = 2.3 and n = 5 showing diaspore-structure phase (d) and unidentified minor phases UG#1 (1) and UG#2 (2) before heating and β-gallia (g) after.

The formation of a continuous solid-solution between GaOOH and MnOOH is reasonable since both have the diaspore-structure phase and their cationic radii are very similar. Trivalent manganese (Mn^{3+}) is smaller than Ga^{3+} (for CN = 6, Ga^{3+} = 0.62 Å vs. Mn^{3+} = 0.58 Å), so it would be expected that the unit cell volumes of α-MnOOH would be smaller than the cell volume of α-GaOOH, however this is not the case. The unit cell volumes are 139.47 $Å^3$ for α-MnOOH and 131.49$Å^3$ for α-GaOOH. This larger unit cell volume for pure MnOOH is attributed to Jahn-Teller distortion in Mn^{3+}.[15,19]

The lattice parameters of the diaspore-structure phases prepared in this study were calculated using α-GaOOH (PDF#06-0180) as the reference structure using the (020), (110), (120), (130), and (111) reflections. Table 3-V compares the measured unit cell volumes to those reported previously.

The measured cell volumes for the diaspore-structure phases prepared in this study were slightly less than those for pure α-GaOOH. This may suggest that no manganese is incorporated into the diaspore-structure, or it may suggest that there is no Jahn-Teller distortion in the solid-solution. There is, however, more significant evidence in the work by Escribano et al.[14] to show that Mn^{3+} does enter the α-GaOOH structure.

Table 3-V. Lattice Parameter Calculations for This Study and Other Relevant Studies.

Composition	Cationic Coordination	a	b	c	Volume (Å^3)	Ref
α-MnOOH	Octahedral	4.554(1)	10.667(1)	2.871(1)	139.47	19
α-GaOOH	Octahedral	4.5171(8)	9.7907(2)	2.9732(4)	131.49	35
α-(Mn,Ga)OOH	Octahedral	n≈5 4.513 n≈9 4.518	9.835 10.066	2.942 2.914	130.6 132.6	14
α-(Mn,Ga)OOH	Octahedral	n=5 4.51(2) n=9 4.51(2)	9.76(2) 9.75(2)	2.96(2) 2.96(2)	130.3 130.2	This study

In this study, the lattice parameters of the diaspore-structure phase in samples prepared with n = 5 and n = 9 are similar. This may suggest that the solubility limit of manganese in the diaspore-structure phase has been exceeded in both compositions. If this were the case, however, one would expect the intensity of the unidentified peaks to be greater in the XRD patters for n = 9 samples, which is not the case. It is interesting to note that Escribano et al.[14] reported that the cell volume of samples prepared with a composition near n = 9 were larger than those prepared with composition n = 5. This trend was not observed in the current study.

Assuming no volatilization has occurred, the lack of a second phase in the x-ray pattern taken after heating at 1000°C suggests that Mn^{3+} is entering the β-Ga_2O_3 structure. This is confirmed by lattice parameter calculations of the β-gallia after heating, where the unit cell volume is 197.6 Å^3, which is about a 6% decrease in size compared to the volume of pure β-Ga_2O_3 (209.5 Å^3). Again, no standard was added to this particular sample, but cell volume of similar compositions showed <0.5% difference between samples with and without internal standard. The formation of a solid-solution is reasonable because β-Ga_2O_3 is known to form extensive solid solutions with Al_2O_3[36] (up to 80% Al^{3+} into β-Ga_2O_3) and In_2O_3[37] (up to 40% In^{3+} into β-Ga_2O_3). The size of the Mn^{3+} and Ga^{3+} ions are also very similar. Escribano et al.[14] reported Mn^{3+} completely entering β-gallia, which is in agreement with this study.

Thermal analysis graphs for sample C4 are given in Figure 3.7. Because the XRD data showed only β-gallia peaks after heating to 1000°C, quantitative analysis of the TGA data was conducted assuming the formation of a beta-gallia solid solution with the composition $Ga_{1.6}Mn_{0.4}O_3$, where it was assumed that all cations added initially are present in the spinel-structure after heating to 1000°C. (For samples prepared as n = 9, the corresponding composition of the β-gallia solid solution is $Ga_{0.88}Mn_{1.12}O_3$). Quantitative calculations show this assumption to be applicable.

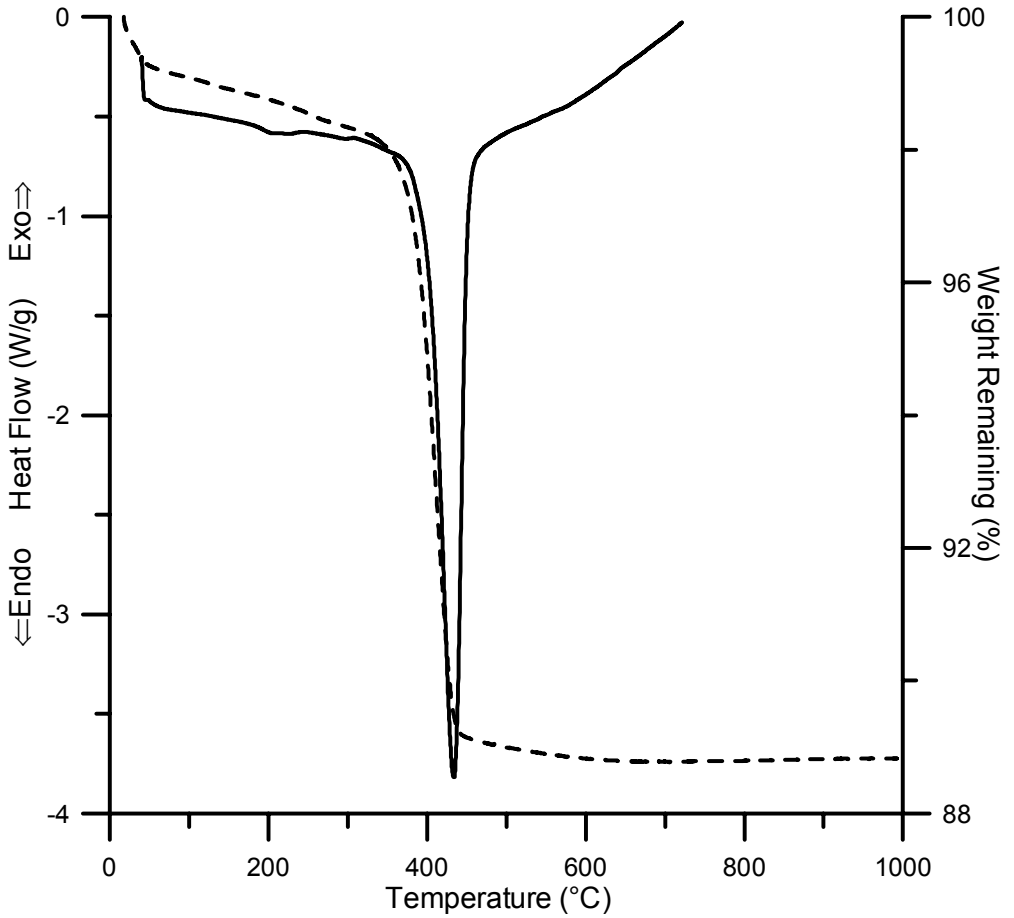

Figure 3.7. Thermal analysis graphs of C4 where TGA is the dashed line and DSC is the solid line.

TGA data of samples containing the diaspore-structure phase and minor unidentified phases showed a slight weight loss at temperatures lower than 400ºC, which is attributed to the loss of absorbed water. Assuming conservation of cations, the final product at 1000ºC is $Ga_{1.6}Mn_{0.4}O_3$. The weight loss below 400ºC corresponds to ~0.05 mol H_2O/mol cation. There was an endothermic process at about 425ºC accompanied by

a weight loss of 0.5 mol H_2O/mol cation, which suggests the following reaction sequence:

$$\alpha\text{-}(Ga_{0.8}Mn_{0.2})OOH \rightarrow \tfrac{1}{2}\, Ga_{1.6}\, Mn_{0.4}O_3 + \tfrac{1}{2}\, H_2O$$

The observed dehydroxlation of (Ga,Mn)OOH occurs at a temperature that is higher than that observed for pure β-gallia. The α-GaOOH to β-Ga_2O_3 transition is reported to occur at 300ºC.[38]

3.3.2.2 Analysis of a Diaspore-Structure and Rutile-Structure Containing Sample

Sample C16 was chosen for further analysis and was dark brown, prepared as n = 9, pH = 6.9 and heated at 225ºC for 19 hours. Figure 3.8 gives the XRD data. After initial processing, XRD data showed a diaspore-structure phase, a rutile-structure phase and UG#2. This was the only sample that showed a rutile-structure phase after drying, and is probably due to the high firing temperature as mentioned earlier. After heating to 1000ºC the sample contained only the spinel-structure phase.

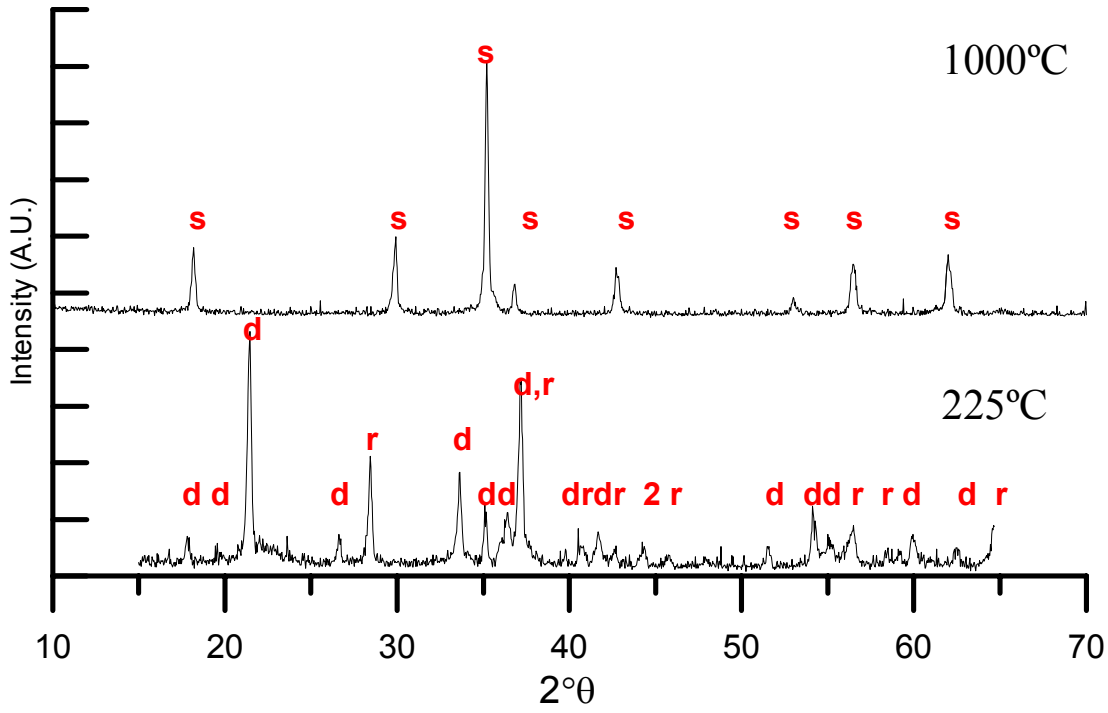

Figure 3.8. XRD data for sample C16 showing a diaspore-structure phase (d) a rutile-structure phase (r) and UG#2 (2) after processing at 225ºC, and a spinel-structure phase (s) after heating to 1000ºC.

Thermal analysis data for C16 are given in Figure 3.9. Initial mole fractions of the diaspore-structure phase and the rutile-structure phase were calculated assuming that the final spinel-structure phase composition was $Ga_{1.33}Mn_{0.66}MnO_4$. The weight loss of 4.8 grams between room temperature and 410ºC was attributed to the loss of water, and the weight loss of 6.8 grams between 410º and 1000ºC was assumed to be due to the loss of oxygen. For the weight loss between 410º and 1000ºC, all the oxygen loss was assumed to be due to the reduction of Mn^{4+} to Mn^{2+}, where all the Mn^{3+} in the β-gallia structure maintained the Mn^{3+} charge during the transformation to the spinel-structure phase. The associated 6.8 grams weight loss was back-calculated to give the amount of Mn^{2+} present at 410ºC. The rest of the manganese present must therefore reside in the Mn^{3+} oxidation state within the diaspore-structure phase along with all of the Ga^{3+}. This then leads to an initial diaspore-structure composition of $Ga_{0.84}Mn_{0.16}OOH$.

The weight loss attributed to water from room temperature to 410ºC corresponds to 0.26 mole H_2O /mole cation in the final spinel-structure phase, which is consistent with the water loss seen in other samples. This loss is reasonable considering there is ½ mole H_2O lost for every mole (Ga,Mn)OOH. The exact mechanism of the O_2 weight loss is

not known. These transitions correspond to 0.20 mole O_2/ mole cation in the final spinel-structure phase. Figure 3.10 gives the detailed attributed weight loss. The proposed reaction sequence is therefore:

$$1.58\ Ga_{0.84}Mn_{0.16}OOH + 1.42\ \beta\text{-}MnO_2 \rightarrow 0.79\ Ga_{1.68}Mn_{0.32}O_3 + 1.42\ \beta\text{-}MnO_2$$
$$+ 0.79\ H_2O\ (g) \rightarrow Ga_{1.33}Mn_{0.66}MnO_4 + 0.61\ O_2\ (g)$$

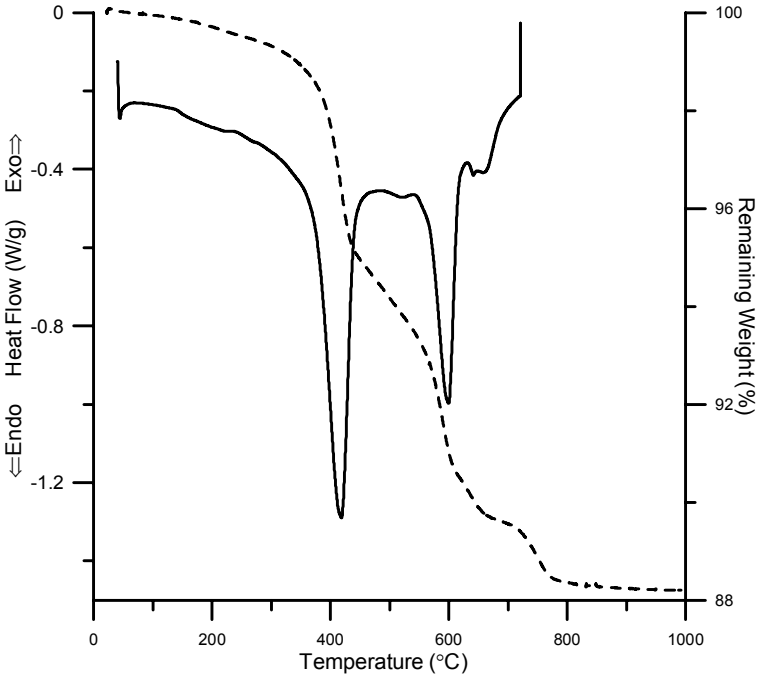

Figure 3.9. Thermal analysis data for sample C16 where the dashed line is TGA data and the solid line is DSC data.

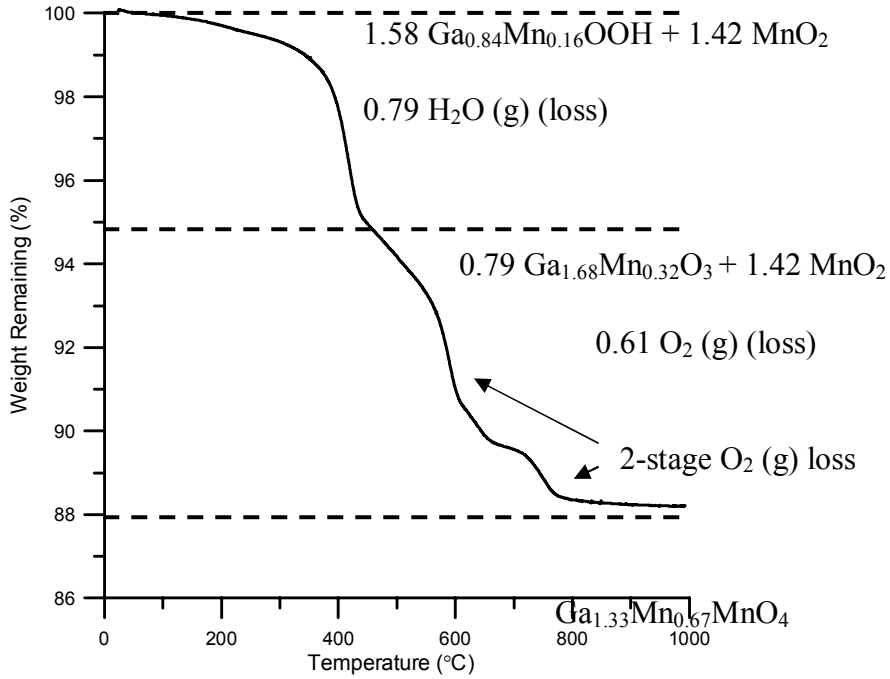

Figure 3.10. TGA data for sample C16 showing attributed weight loss and proposed compositions.

3.3.2.3 Analysis of a Spinel-Structure and Bixbyite-Containing Sample

Sample C18 was selected for further analysis and was dark brown, prepared as n = 9, pH = 8.7 and heated at 230ºC for 19 hours. After drying, XRD data showed a spinel-structure phase and maybe orthorhombic-bixbyite, as given in Figure 3.11.

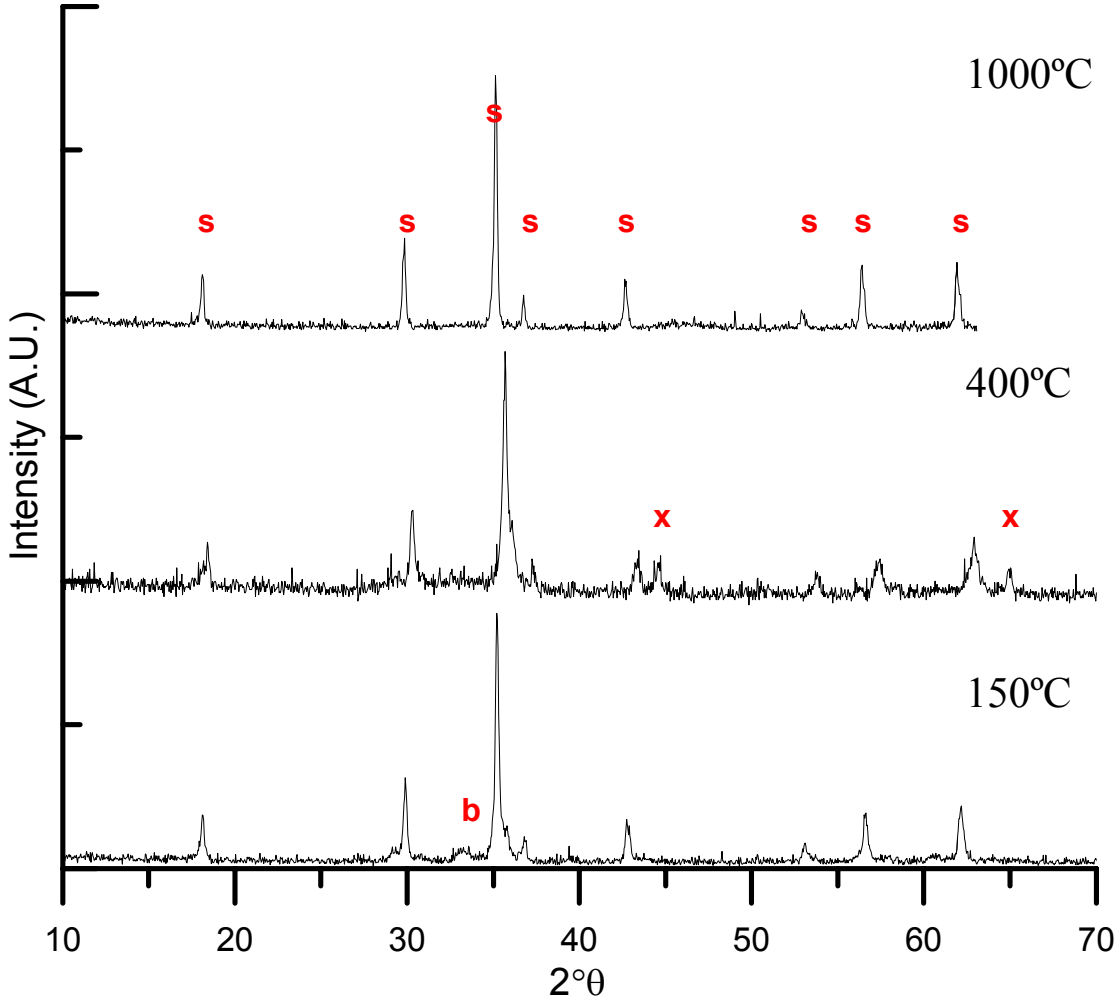

Figure 3.11. XRD data for sample C18 containing a spinel-structure phase (s) and maybe bixbyite (b) at 150ºC, where the phase in the sample transforms to a spinel-structure phase and unidentified phase PG x (x) appearing at 400ºC. Unidentified phase PG x and a spinel-structure phase are transforming to only a spinel-structure phase before 1000ºC.

Lattice parameters for samples containing a spinel-structure phase after drying were calculated using the (111), (220), (311) and (440) peaks. Not all samples were mixed with an internal standard; however, the difference in lattice parameter calculations

between samples with and without a standard was <0.5%. Table 3-VI gives the unit-cell volume previously reported for the two spinel-structure phases and the average unit-cell volume of the spinel-structure phase for samples prepared as n = 9.

Table 3-VI. Cell Volume Data for This Study and Other Relevant Studies.

Composition	Lattice Volume ($Å^3$)	Reference
Ga_2MnO_4	605	31
$Ga_{1.334}Mn_{0.66}MnO_4$ (n=9)	602.6[9]	This study
Mn_3O_4	596.95	28

Samples were prepared as n=9, with initial cation mole fractions of 0.44 moles Ga^{3+} for every 0.55 moles Mn^{3+}, thus complete dissolution of cations into the spinel-structure phase would yield a spinel-structure phase composition expressed as $(Ga_{1.334}Mn_{0.666})^{3+}Mn^{2+}O_4$. Because the mole fraction of manganese in n = 9 is in between the mole fraction of manganese in Ga_2MnO_4 and Mn_3O_4, the unit cell volume of n = 9, assuming full dissolution of the cations into the spinel-structure phase, should also be in between these two volumes, which is the case in this study.

This formula $Ga_{1.334}Mn_{0.666}MnO_4$ was used to determine the amount of cation participating in a reduction reaction for calculating the theoretical weight loss of a sample showing only the spinel-structure phase. In samples where there was more than one phase, it was not possible to determine how much cation substitution occurred among the phases. Because of this uncertainty, it was not possible to determine the theoretical weight loss.

The x-ray diffraction pattern of samples heated to 1000ºC corresponded to the pattern for a spinel-structure phase. TGA and DSC data are given in Figure 3.12. The XRD data from the dried sample correspond to the powder diffraction file entry for a spinel-structure phase, but with an additional peak at about 33.5º2θ. This peak corresponds to the highest intensity peak (222) in orthorhombic bixbyite. Upon heating, there is a weight loss of 3.7% and an endotherm from 35º-200ºC. There is also an apparent exothermic process occurring around 200ºC. It is important to note that this exotherm is small in comparison to that shown for the sample containing only the diaspore-structure phase. This exotherm could merely be the recovery to zero from the

[9] Average value of two samples, with a standard deviation of 1.68.

previous endotherm. Weight loss at this temperature range is typical of dehydroxylation. However, the x-ray diffraction patterns of the dried sample did not show any hydroxide or oxyhydroxide phases. If the transition were exothermic, it could be associated with the reactions to form the unidentified phase observed in the 400ºC XRD pattern, i.e. the peaks designated PG x. The DSC peak at about 275ºC is assumed to be the recovery to the zero point, and not an exotherm.

Another weight loss and associated endothermic process occurs around 600ºC. The XRD data at 1000ºC correspond to a pure spinel-structure phase. The weight loss near 600ºC corresponds to 0.07 mole O_2/mole Mn^{2+} in the final spinel-structure product. The associated transition is:

$$2/3\ Ga_2MnO_4 + 1/2\ Mn_2O_3 \rightarrow (Ga_{1.334}Mn_{0.666})^{3+}Mn^{2+}O_4 + 1/12\ O_2(g)$$

This transition is in good agreement with the theoretical weight loss of 0.08 mole O_2 loss/ mole Mn^{2+}. The source of weight loss near ~200ºC could not be determined in this study. It is possible that it is associated with the loss of absorbed water and that an exothermic reaction, associated with the formation of the unidentified phase, "masked" the endothermic process associated with the loss of absorbed water. If the first weight loss step were attributed to water, it corresponds to about 0.18 mole H_2O/ mole cation in the final spinel-structure product. However, there is no evidence in the initial x-ray pattern as to the location of this water. A summary of the proposed transitions is given as Figure 3.13.

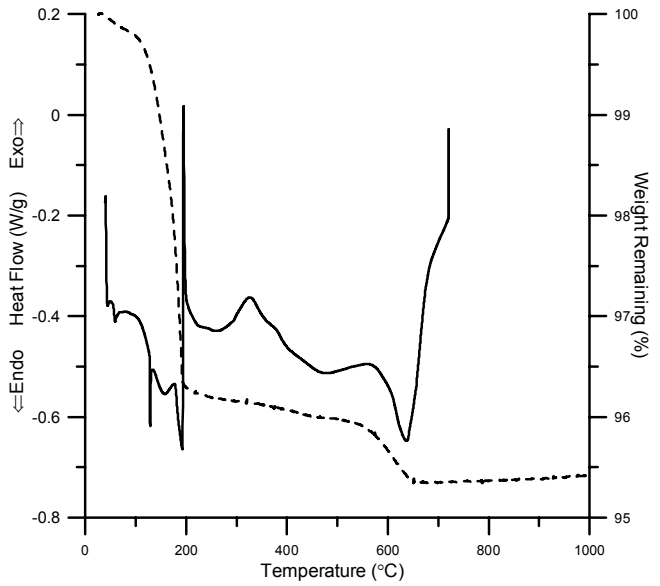

Figure 3.12. Thermal analysis data for sample C18 where the dashed line is TGA data and the solid line is DSC data.

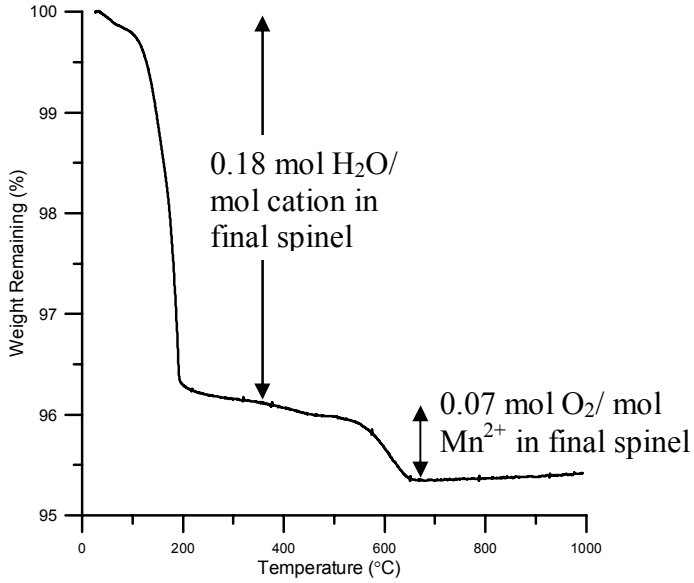

Figure 3.13. TGA data for sample C18 showing proposed transitions.

3.3.2.4 Analysis of a Spinel-Structure and Diaspore-Structure-Containing Sample

Sample C7 was chosen for further analysis and was prepared as n = 5, pH = 9.8 and heated to 230ºC for 19 hours. After drying, the sample was dark brown. The XRD pattern peaks, corresponding to the spinel-structure and the diaspore-structure, were broad, perhaps indicating a sample that was poorly crystallized and not completely reacted.

The only difference between the samples C7 and C18 was the n-value. Therefore, it is assumed the higher manganese content in the C18 sample (prepared as n = 9) promoted the formation of bixbyite.

The XRD and thermal analysis data for C7 are given as Figure 3.14 and Figure 3.15. The sample undergoes a series of weight loss steps from room temperature to 1000ºC. Because the weight vs. temperature curve does not level off at 1000ºC, any calculations based on assumptions regarding the final product will have some degree of error. Nevertheless, if one assumes that the final product contains Ga_2MnO_4 and Ga_2O_3 in a one-to-one molar ratio, one possible corresponding chemical reaction is as follows:

$$2GaOOH + Ga_2MnO_4 \rightarrow Ga_2O_3 + H_2O + Ga_2MnO_4$$

This reaction assumes that Ga_2MnO_4 is the composition of the spinel-structure phase observed after drying. The total weight loss associated with this reaction would be around 3.7 grams, which is much lower than observed. Moreover, the weight loss near 600ºC is similar to the weight loss observed for the reduction of manganese.

Another possible reaction, which assumes that the spinel-structure observed after drying is Mn_3O_4, and can be written as follows:

$$4\ GaOOH + 1/3\ Mn_3O_4 \rightarrow Ga_2O_3 + Ga_2MnO_4 + 2\ H_2O + 1/6\ O_2(g)$$

The total weight loss associated with this reaction would be about 8.5 grams, which is greater than that observed. Partial substitution of Ga^{3+} for Mn^{3+} in the Mn_3O_4 and partial substitution of Mn^{3+} for Ga^{3+} in GaOOH would result in a weight loss between 3.7 and 8.5 grams.

The DSC data show broad endothermic peaks over the entire temperature range and a sharp exotherm at about 140ºC. Dehydroxylation and reduction are both endothermic processes. The sharp exotherm may be associated with crystallization of the poorly crystallized starting powders.

The two stage weight loss is therefore uncertain. The first weight loss from room temperature to about 600ºC is probably due to a loss in water, and the second weight loss from 600º to 1000ºC is probably due to a reduction reaction, however, because the reaction was not complete, and the location of these cations is unknown, theoretical weight loss calculations could not be conducted with any certainty.

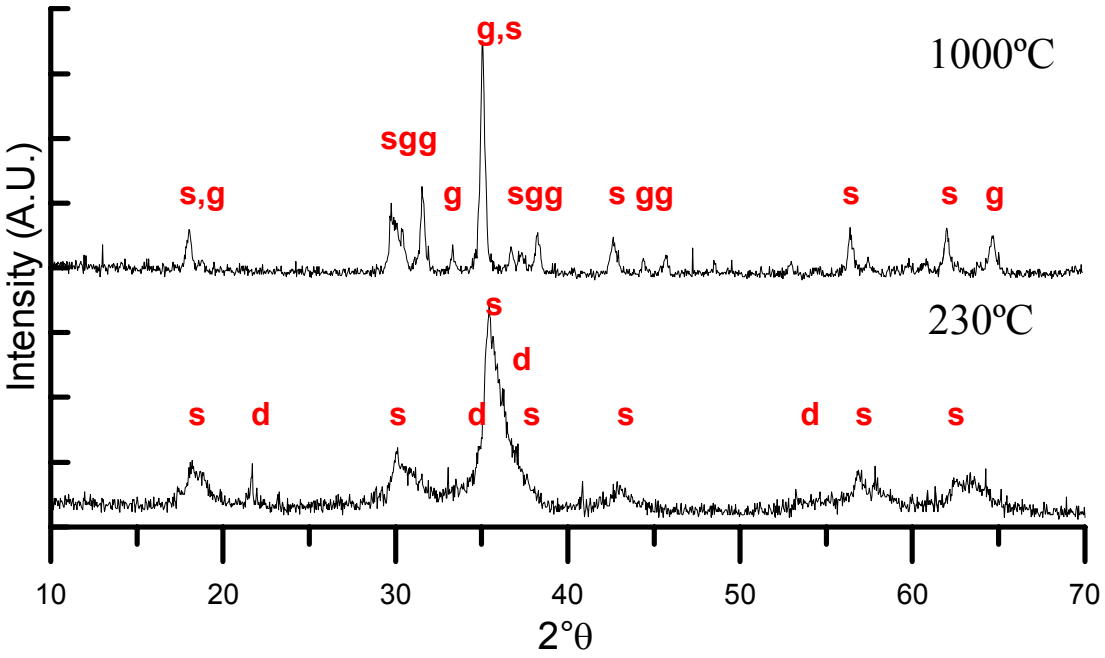

Figure 3.14. XRD data for sample C7 prepared with n = 5 and pH = 9.8 showing a poorly crystallized spinel-structure phase(s) and a diaspore-structure phase (d) after drying. After heating to 1000ºC, the sample shows a spinel-structure phase and a β-gallia-structure phase(g).

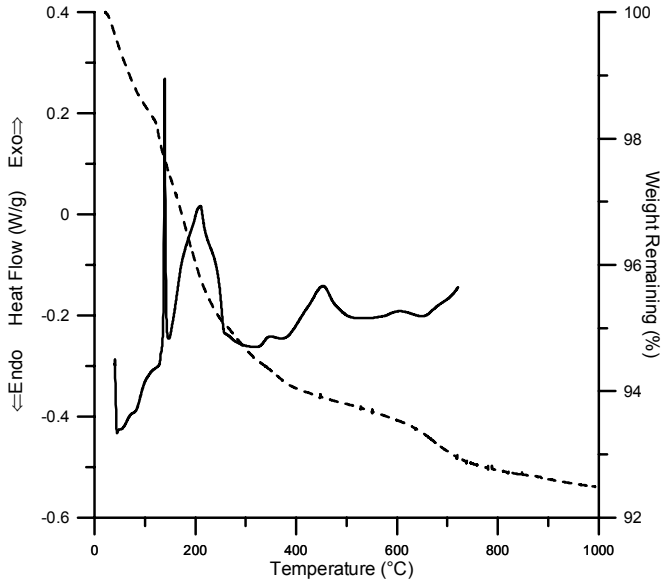

Figure 3.15. Thermal analysis data for sample C7 where the dashed line is TGA and the solid line is DSC.

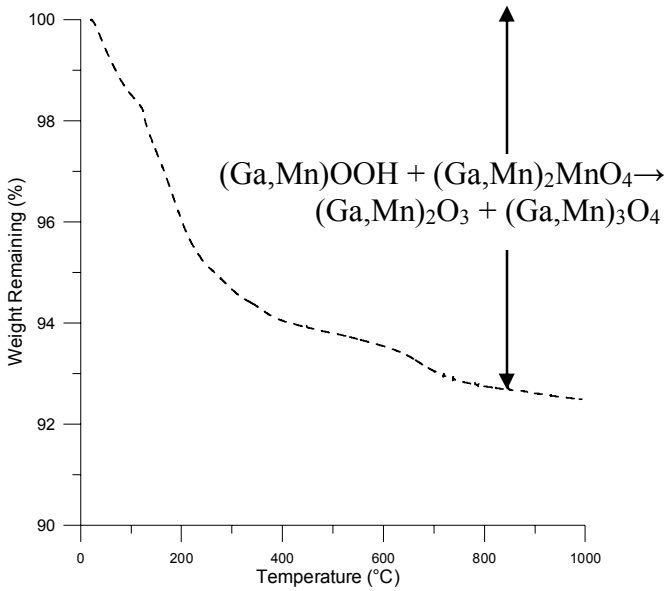

Figure 3.16. TGA data for sample C7 showing proposed transition.

3.3.2.5 Analysis of Unidentified Major Phases

Samples with unidentified major phases UA, UB and UC were studied in detail. The x-ray patterns of these samples after drying were compared to the powder diffraction file entries in Table 3-III and generated intergrowth patterns in Figure 3.3; there were no apparent matches. TGA and DSC experiments were performed, and based on these data, transitions were proposed. The same difficulties arose with the uncertainty of cation location in the previous analyses, where in the analysis of these unidentified major phases, less information is available from XRD. Weight losses were calculated according to a mixed stoichiometry, i.e. $(Ga_{1.334}Mn_{0.666})Mn_2O_4$ for n = 9, calculated by considering the original stoichiometry (0.55 mole ratio gallium for n = 9 vs. 0.80 for n = 5). This, of course, cannot take into consideration the composition of any other undetectable phases. The appearance and disappearance of peak groups were analyzed as a function of temperature.

Sample C19 was prepared as n = 9 with pH = 9.3, heated to 150ºC for 19 hours. The sample was dark brown and contained UB. XRD data are given in Figure 3.17 and thermal analysis data are given in Figure 3.18. The XRD data suggest that UB undergoes a phase transition or reaction between 150º and 270ºC, with the possible formation of phase i. The thermal analysis data in R2 show that an endothermic process and significant weight loss occur over the temperature range of R2. The XRD pattern at 500ºC shows the emergence of peaks associated with the spinel-structure phase. TGA data show a weight decrease at about 650ºC (R4), in agreement with the expected weight change on the formation of the spinel-structure phase. The XRD data at 900ºC show the spinel-structure phase, and bixbyite, where quantitative weight loss calculations are done assuming the composition $Ga_{1.33}Mn_{0.667}MnO_4$. The formation of the spinel-structure phase likely involves the reduction of Mn^{3+} to Mn^{2+}, which can be expressed as:

$$2\ Mn^{3+} + 3\ O^{2-} \rightarrow 2\ Mn^{2+} + 2\ O^{2-} + \tfrac{1}{2}\ O_2\ (g)$$

If one assumes that final composition of the spinel-structure phase at 900ºC is $Ga_{1.33}Mn_{0.667}MnO_4$, and cation mass is conserved, the weight loss associated with the

reaction above 500ºC would be about 2.8 grams. This suggests that the two endotherms at 300ºC and 600ºC are associated with the reduction process.

The endothermic process occurring around 200ºC is thought to be associated with a dehydroxylation process, which can be expressed generically as:

$$0.88\ Ga^{3+} + 1.11\ Mn^{3+} + 2\ O^{2-} + 2\ OH^{-} \rightarrow 0.88\ Ga^{3+} + 1.11\ Mn^{3+} + 3\ O^{2-} + H_2O$$

Assuming again that the final composition of the spinel-structure phase at 900ºC is $Ga_{1.33}Mn_{0.667}MnO_4$, and that the cationic mass is conserved, the weight loss associated with the dehydroxylation reaction would be about 9.5 grams and corresponds to about 0.49 mole H_2O/ mole cation; this is reasonable based on the TGA results and the suggested transition. The remaining weight loss below 100ºC is likely due to absorbed water of about 0.08 mol H_2O/mol cation, similar to that acquired for sample C7. A summary of proposed transitions is given as Figure 3.19.

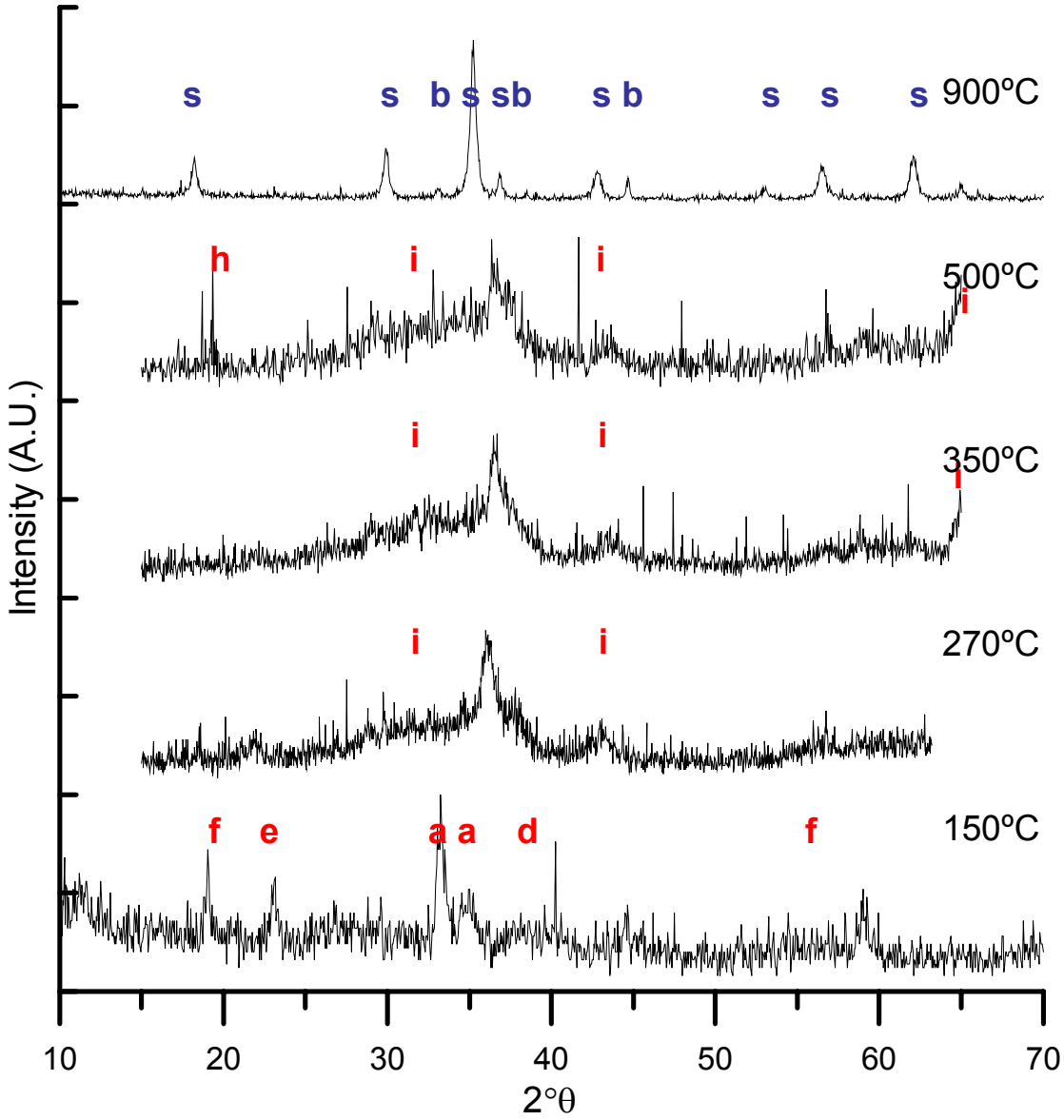

Figure 3.17. XRD data for sample C19 with UB after drying.

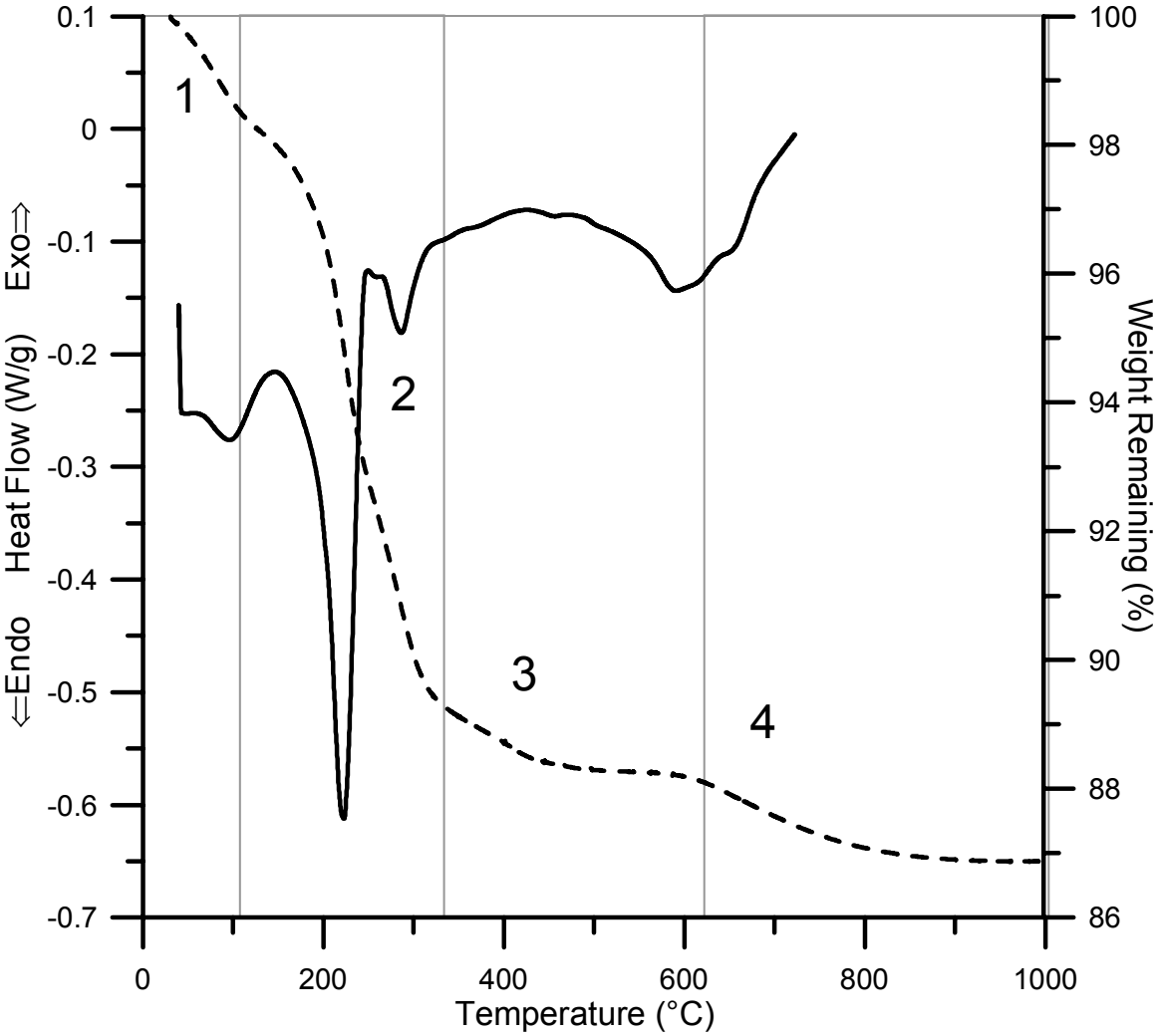

Figure 3.18. Thermal analysis data for C19 with UB where the dashed line is TGA data and the solid line is DSC data.

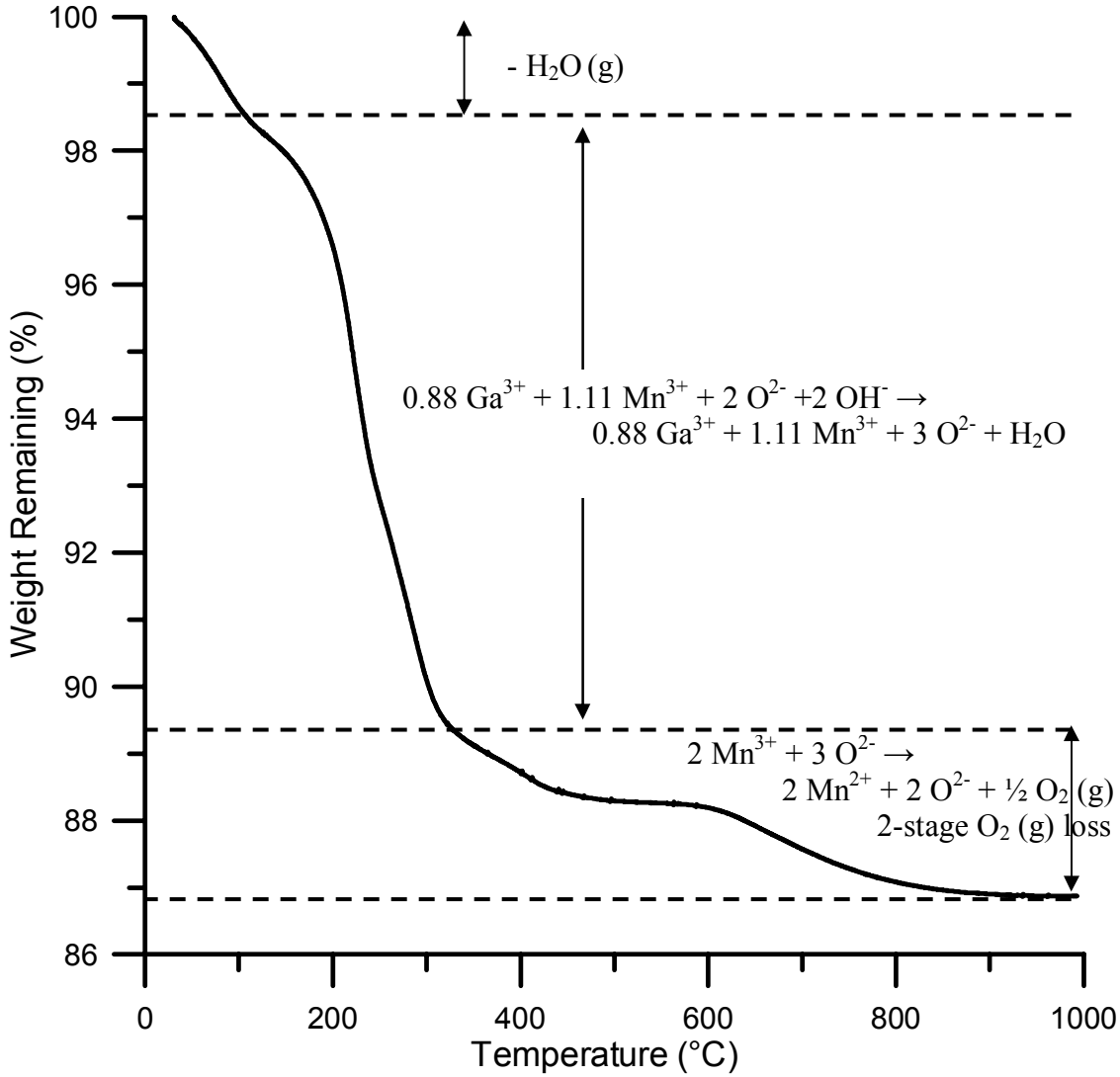

Figure 3.19. Summary of the proposed reactions for C19 shown with the TGA data.

Sample C21 was prepared with n = 9, pH = 9.6 and heated to 150ºC for 65 hours. After drying it was dark brown and contained UA. X-ray diffraction and thermal analysis data are given in Figure 3.20 and Figure 3.21, respectively. After heating to 1000ºC, the diffraction pattern for the sample shows a spinel-structure phase and peaks that may correspond to bixbyite-structure phase.

The XRD data in R2 shows the disappearance of phase f and the emergence of phase c. Thermal analysis data shows an endothermic process and associated weight loss occurring in this region. In R3, there is a transition of c, a and d to form an unidentified phase i. There is an exotherm in this region associated with a weight loss, which is

consistent with this transition. In R4 and R5 the sample transforms to the spinel-structure phase, with an associated weight loss at about 700ºC. The weight loss associated with R4 and R5 is believed to be associated with the reduction of Mn^{3+} to Mn^{2+}, according to the reaction:

$$2\ Mn^{3+} + 3\ O^{2-} \rightarrow 2\ Mn^{2+} + 2\ O^{2-} + \tfrac{1}{2}\ O_2\ (g)$$

However, if one assumes that the final composition of the spinel-structure phase at 900ºC as $Ga_{1.33}Mn_{0.667}MnO_4$ and that cation mass is conserved, the weight loss associated would be about 2.9 grams, which is considerably lower than that observed for the R4 and R5 region. This suggests that some manganese is in the divalent state at temperatures lower than 350ºC. This then also suggests that the exothermic reaction near 300ºC in R3 results in the formation of the phase with divalent manganese. Because there is little information about the composition of the unidentified phases, it is difficult to interpret the TGA data at lower temperatures. However, based on the data from UB and other samples, it is likely that the weight loss in R1 and R2 is due to the loss of water. This weight loss in R1 and R2 corresponds to 0.25 mole H_2O/ mole cation in the final spinel-structure product. The weight loss during R3 may be a combination of water and oxygen loss.

The data from C21 with UA are similar to data from C19 with UB. This phase f and the transition temperature are similar in UA and UB; however, phase e is only present in UB. Phase a appears to be the same in both samples. The transition of a and d to form unidentified phase i occurs between 250º and 270ºC. Both show the transformation of phase b to spinel-structure between 500º and 900ºC.

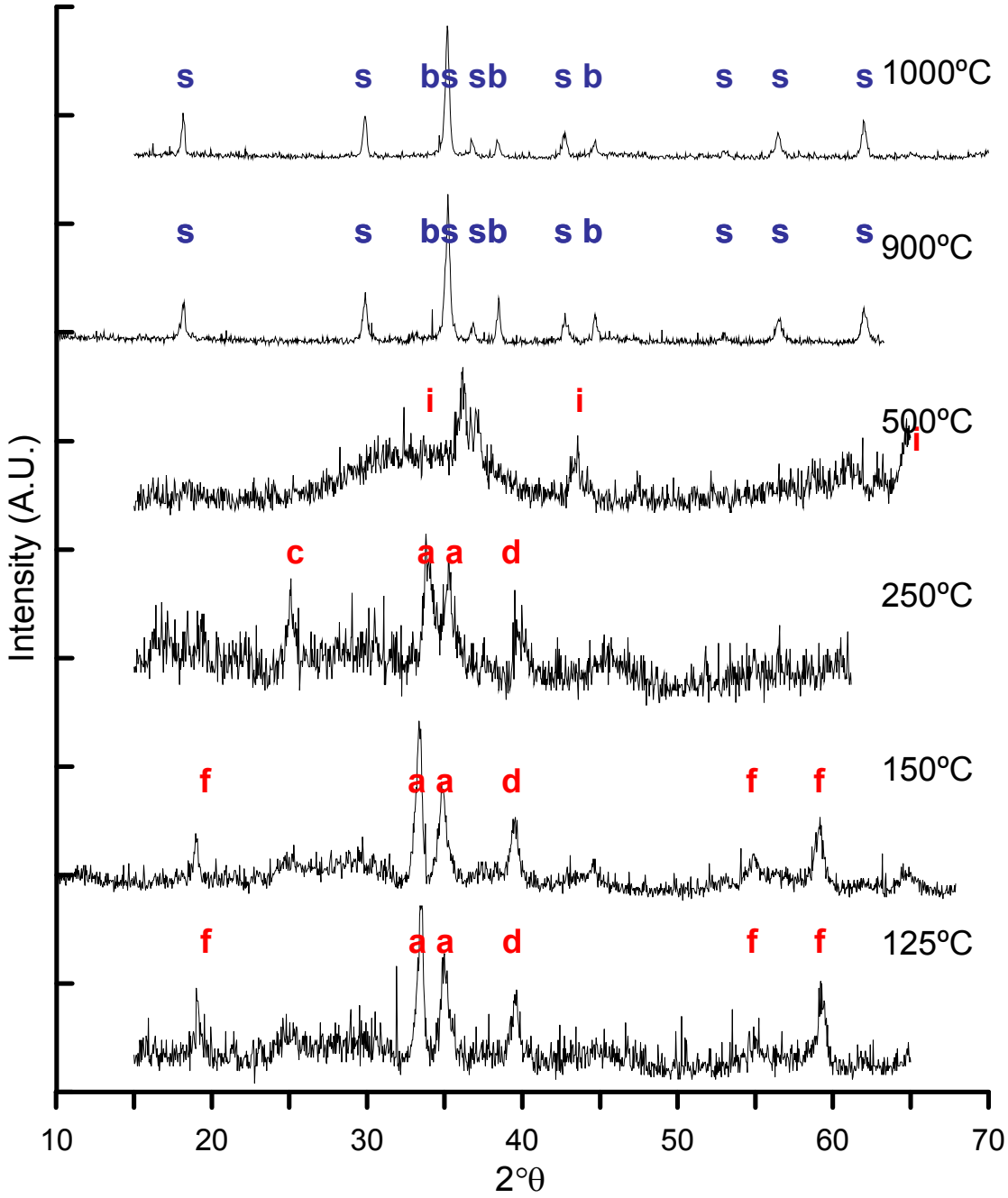

Figure 3.20. XRD data for sample C21 with UA after drying. The sample showed a spinel-structure phase (s) and maybe bixbyite-structure phase (b) after heating to 900ºC.

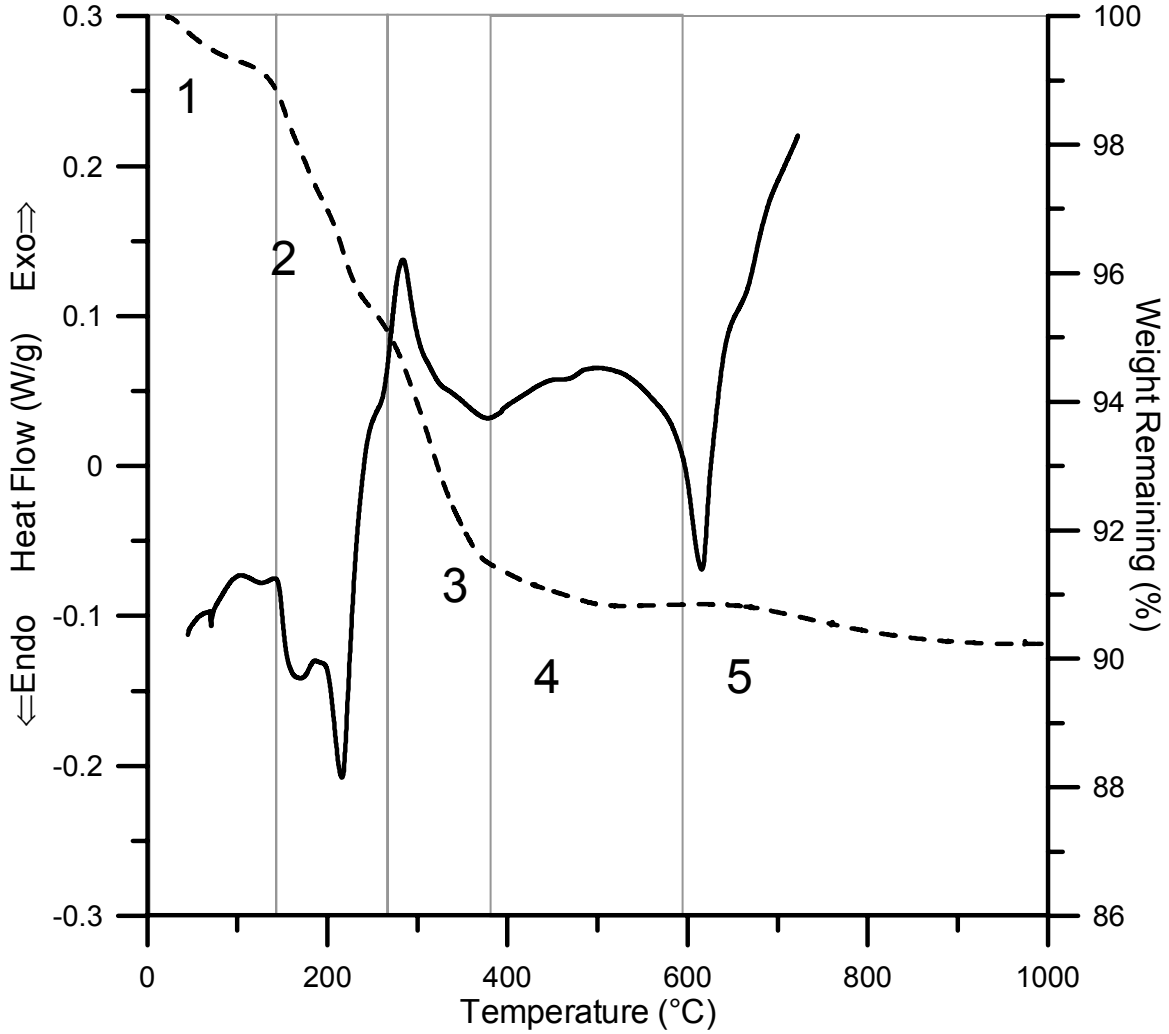

Figure 3.21. Thermal analysis graph for C21 with UA where the dashed line is TGA data and the solid line is DSC data.

TEM was conducted on UA and UB, where the micrograph of UA is given in Figure 3.22. Both UA and UB showed plate-like particles, square-shaped particles and two types of elongated crystals. EDS was conducted and showed the plate-like crystals, the square-shaped crystals and the thicker-rod shaped crystals contained Ga, Mn and O, and the more needle-like crystals contained Mn and O. The rod-shaped crystals were similar in shape to the crystals previously reported for α-GaOOH.[17] UB showed similar data, although there were a greater number of elongated particles. This limited analysis suggests that UB contains UA and that the initial compositions were only slightly different. This also provides evidence that there may be a preferred orientation on the

sample holders because of these morphologies, perhaps explaining the difficulty in identifying x-ray data.

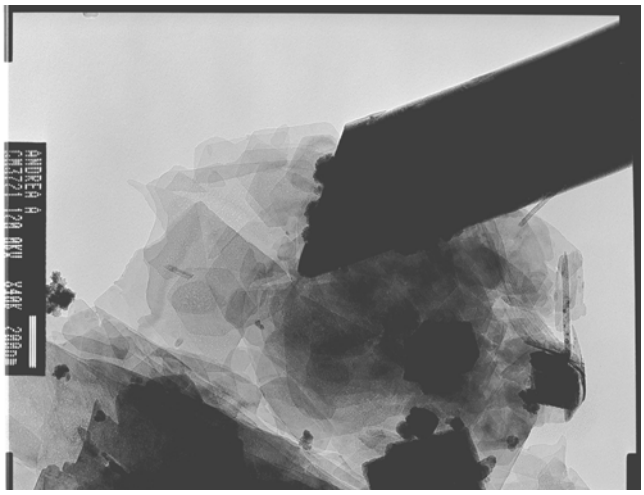

Figure 3.22. TEM of UA powder showing elongated crystals and square-shaped crystals.

Jahn-Teller (JT) distortion in manganese causes changes in x-ray patterns. Figure 3.23 demonstrates the difference in x-ray patterns between the isostructural α-GaOOH and α-MnOOH, with the latter showing this effect. It is therefore difficult to characterize samples according to x-ray patterns. Also, lattice parameters are affected by JT distortion, so proving the existence of cation substitution is difficult. Unidentified minor and major phases could be intergrowths of known phases, which would yield new, unrelated x-ray patterns. TGA and DSC could only give possible transitions but could not confirm data.

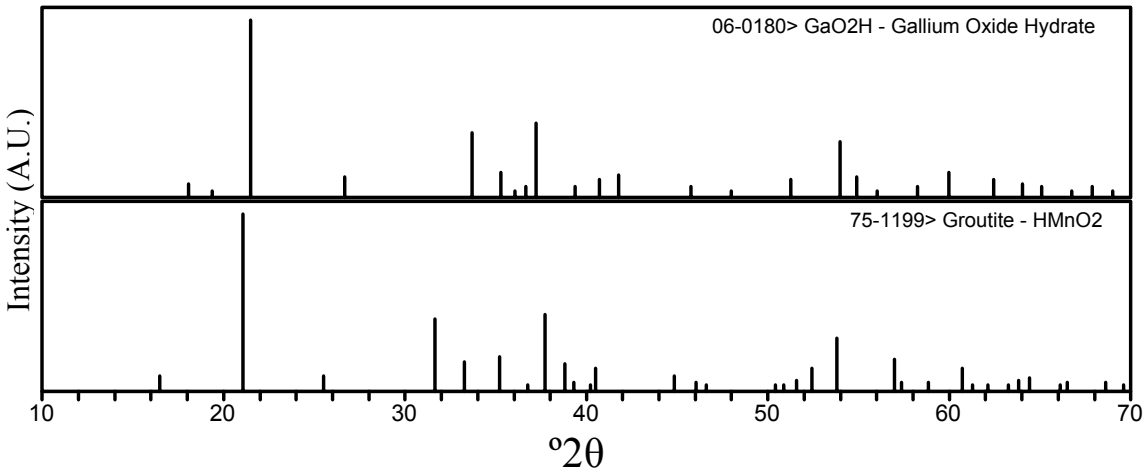

Figure 3.23. PDFs of isostructural oxyhydroxides showing the drastic affect Jahn-Teller distortion has on diffraction patterns.

Sample C22 was prepared as n=9, pH=9.6 and heated to 180ºC for 19 hours. After drying, the sample was dark brown and contained UC. After heating to 1000ºC, the sample contained a spinel-structure phase. XRD data are given in Figure 3.24 and thermal analysis data is given as Figure 3.25.

There are four distinct weight loss events. XRD data show the transformation of phases t and m and the appearance of phases j and n between 180º and 300ºC. Thermal analysis data in R1 and R2 show a sharp exotherm at about 190ºC. The peaks in phases k and q appear to be merely shifted from each other, meaning they may be a related phase. There is no change in the XRD patterns between 300º and 425ºC, which is fairly consistent with the lack of any thermal events. XRD data of the sample at 900ºC corresponds to the spinel-structre phase being present. R3 and R4 are believed to be associated with the reduction of Mn^{3+} to Mn^{2+} according to the reaction:

$$2\ Mn^{3+} + 3\ O^{2-} \rightarrow 2\ Mn^{2+} + 2\ O^{2-} + \tfrac{1}{2}\ O_2\ (g)$$

If one assumes that the final composition of the spinel-structure phase at 900ºC is $Ga_{1.333}Mn_{0.667}MnO_4$, and cation mass is conserved, the weight loss associated with the reaction above would be about 2.9 grams, which is in good agreement with the TGA data. Because there is little information about the composition of the unidentified phasess, it is difficult to interpret the TGA data at temperatures lower than 350ºC. The transition may be associated with a loss of water and/or O_2.

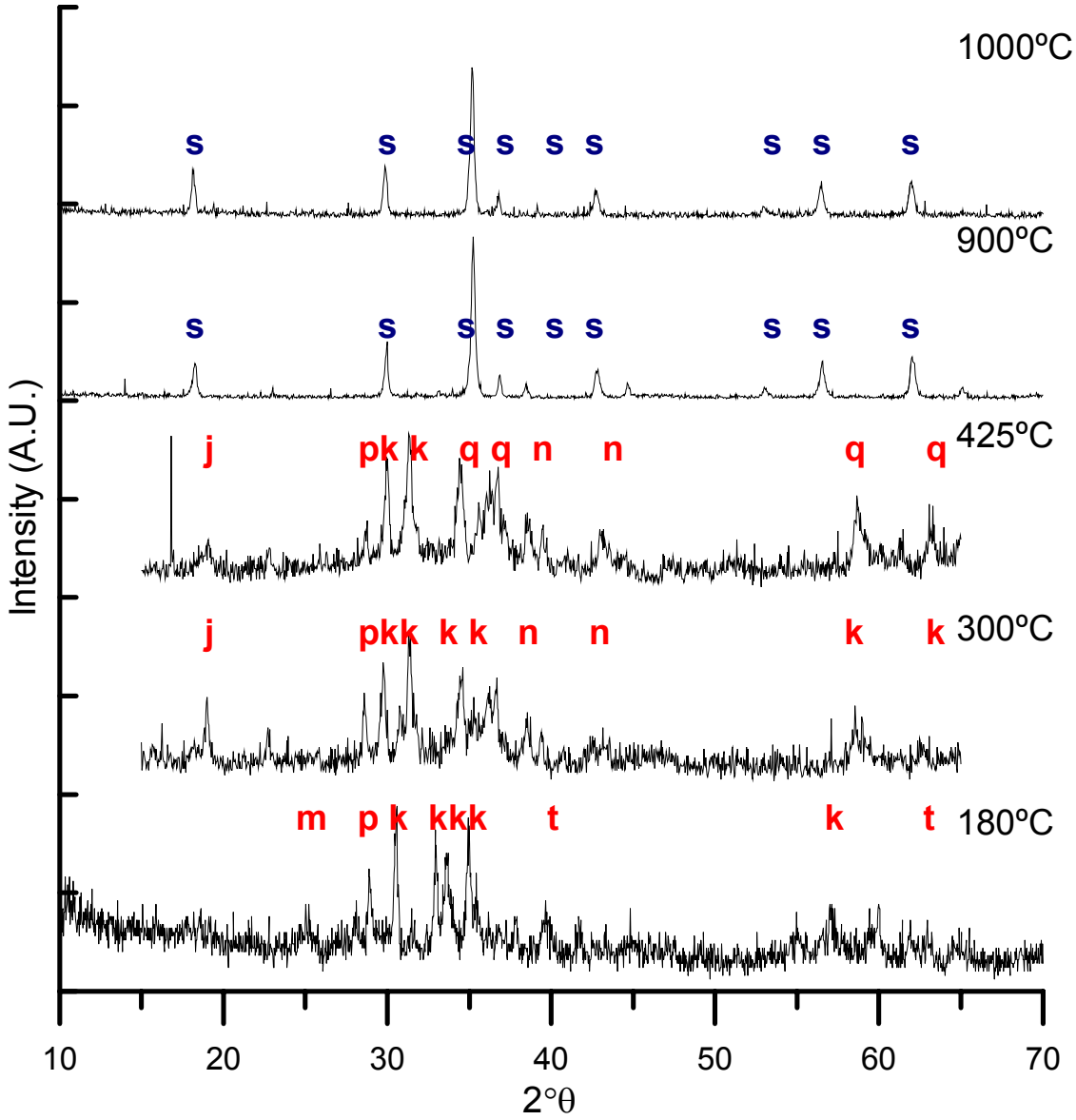

Figure 3.24. XRD data from sample C22 shows the presence of the phase UC after drying and spinel-structure phase after heating to 900ºC.

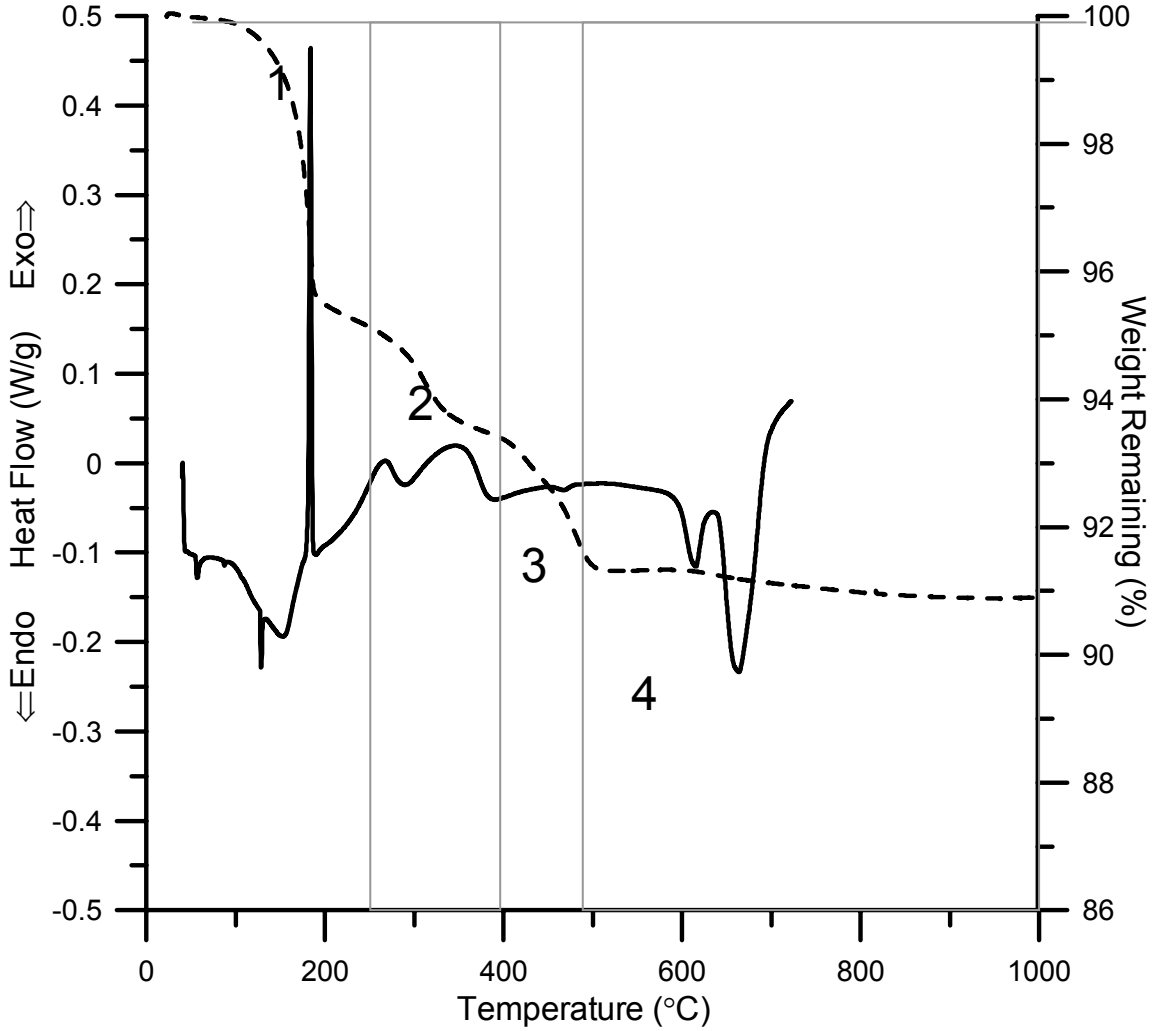

Figure 3.25. Thermal analysis data for sample C22 with UC after drying and spinel-structure phase after heating to 900ºC.

3.4 Conclusions

General results show regions of phase stability for gallium-manganese oxides as a function of processing temperature and pH. A solid solution of gallium and manganese in the diaspore-structure phase is stable for all temperatures where the starting pH < 7. Generally, where the starting pH > 7, a solid solution of the spinel-structure phase is stable. Four samples with pH > 9 and processing temperatures less than 170ºC contained major unidentified phases. Minor unidentified phases were dependant on processing temperature. The heating time had little if any affect on the results.

Some results of this study were in agreement with the study by Escribano et al.[14] Manganese has shown to be incorporated into the diaspore-structure phase, the spinel-structure phase and β-gallia structure.

The most frequently observed phase was the diaspore-structure phase, which was observed over the entire composition and pH range, depending on processing method. In this study, the addition of smaller Mn^{3+} ions for Ga^{3+} ions decreases the size of the diaspore-structure phase with no sign of Jahn-Teller distortion. In order to attain the diaspore-structure phase (with Mn^{3+}) from the addition of rutile-structure form of manganese (Mn^{4+}), there must be a reduction and endothermic reaction, as seen in the thermal analysis data. In both phases manganese is in octahedral coordination. The bond lengths of manganese-substituted diaspore should be studied further.

Manganese oxide in the stoichiometry Mn_2O_3 forms bixbyite (either cubic or orthorhombic, depending on the temperature), but not a β-gallia structure. However Mn^{3+} will enter the β-gallia structure. This is reasonable because of the close size of the cations and the ability of gallium to form extensive solid solutions with similar cations.

The formation of a spinel-structure solid solution is reasonable since the spinel-structure is known to form with the stoichiometry of Ga_2MnO_4 and Mn_3O_4. For samples prepared as n = 5 (more Ga^{3+} than Ga_2MnO_4), higher temperatures are required to attain the spinel-structure than for samples with a lower initial Ga^{3+} content such as n = 9.

Because unidentified phases were not reported in the Escribano et al.[14] study, new phases may be a product of the hydrothermal synthesis processing conditions. Unidentified major phases all transform to the spinel-structure after heating above 900ºC. Thermal analysis was unable to conclude any specific reactions.

The results were somewhat dependent on the processing method. Microwave hydrothermal synthesis showed both different and repeated results compared to conventionally prepared samples. More specifically, microwave hydrothermal synthesis appears to promote the formation of UG #3 at low pH and discourages the formation of diaspore-structure phase at higher pH.

Further study on the location of manganese within these structures is needed, in addition to further analysis of unknown phases.

3.5 References

1. M.M. Thackeray, "Manganese Oxides for Lithium Batteries," *Prog. Solid State Chem.,* **25** [1] 1-71 (1997).

2. C. Klingsberg and R. Roy, "Solid-Solid and Solid-Vapor Reactions and a New Phase in the System Mn-O," *J. Am. Ceram. Soc.,* **43** [12] 620-6 (1960).

3. J.P. Coughlin, "Data on Theoretical Metallurgy: XII Heats and Free Energies of Formation of Inorganic Oxides," *U.S. Bur. Mines Bull.,* **542** [1] 80 (1954).

4. E.P. Tatievskaya, G.I. Chufarov, V.K. Antone, and "Kinetics of Reduction and Dissociation of Manganese Oxides, Vol. I*zvest. Akad. Nauk SSSR Otdel. Nauk*, 371-83 (1948). As cited in C. Klingsberg and R. Roy, "Solid-Solid and Solid-Vapor Reactions and a New Phase in the System Mn-O," *J. Am. Ceram. Soc.*, 43 [12] 620-6 (1960).

5. G.W. Morey, "Hydrothermal Synthesis," *J. Am. Ceram. Soc.,* **36** [9] 279-85 (1953).

6. M.N. Rahaman, *Ceramic Processing and Sintering;* pp. 69-71. Marcel Dekker, NY, 1995.

7. Y.C. Zhang, H. Wang, H.Y. Xu, B. Wang, H. Yan, A. Ahniyaz, and M. Yoshimura, "Low-Temperature Hydrothermal Synthesis of Spinel-Type Lithium Manganese Oxide Nanocrystallites," *Solid State Ionics,* **158** [1/2] 113-7 (2003).

8. M.S. Whittingham, "Hydrothermal Synthesis of Transition Metal Oxides under Mild Conditions," *Curr. Opin. Solid State Mater. Sci.,* **1** [1] 227-32 (1996).

9. G.W. Morey and P. Niggli, "The Hydrothermal Formation of Silicates, A Review," *J. Am. Chem. Soc.,* **35** [9] 1086-130 (1913).

10. J.J. Xu and J. Yang, "Nanostructured Amorphous Manganese Oxide Cryogel as a High-Rate Lithium Intercalation Host," *Electrochem. Commun.,* **5** [3] 230-5 (2003).

11. O.P. Bricker, "Some Stability Relations in the System Mn-O_2-H_2O at 25°C and One Atmosphere Total Pressure," *Am. Mineral.,* **50** [9] 1296-354 (1965).

12. R. Roy, V.G. Hill, and E.F. Osborn, "Polymorphism of Ga_2O_3 and the System Ga_2O_3-H_2O," *J. Am. Ceram. Soc.,* **74** [2] 719-22 (1952).

13. R.S. Zhou and R.L. Snyder, "Structures and Transformation Mechanisms of the ε, γ and θ Transition Aluminas," *Acta Crystallogr.,* **B 47** [5] 617-30 (1991).

14. V.S. Escribano, E.F. Lopez, P.S. Huidobro, M. Panizza, C. Resini, J.M. Gallardo-Amores, and G. Busca, "Characterization of Manganese-Gallium Mixed Oxide Powders," *Solid State Sci.,* **5** [11/12] 1481-9 (2003).

15. L.S.D. Glasser and L. Ingram, "Refinement of the Crystal Structure of Groutite, α-MnOOH," *Acta Crystallogr.,* **B 24** [9] 1233-36 (1968).

16. A.W. Laubengayer and H.R. Engle, "The Sesquioxide and Hydroxides of Gallium," *J. Am. Chem. Soc.,* **61** [5] 1210-14 (1939).

17. A.C. Tas, P.J. Majewski, and F. Aldinger, "Synthesis of Gallium Oxide Hydroxide Crystals in Aqueous Solutions with or without Urea and Their Calcination Behavior," *J. Am. Ceram. Soc.,* **85** [6] 1421-29 (2002).

18. T. Hatakeyama and Z. Liu, *Handbook of Thermal Analysis*. John Wiley & Sons, West Sussex, England, 1998.

19. T. Kohler, T. Armbruster, and E. Libowitzky, "Hydrogen Bonding and Jahn-Teller Distortion in Groutite, α-MnOOH, and Manganite, γ-MnOOH, and Their Relations of the Manganese Dioxides Ramsdellite and Pyrolusite," *J. Solid State Chem.,* **133** [2] 486-500 (1997).

20. P.K. Sharma and M.S. Whittingham, "The Role of Tetraethyl Ammonium Hydroxide on the Phase Determination and Electrical Properties of γ-MnOOH Synthesized by Hydrothermal," *Mater. Lett.,* **48** [6] 319-23 (2001).

21. H.F. McMurdie and E. Golovato, "Study of the Modifications of Manganese Dioxide," *J. Res. Natl. Bur. Stand. (U.S.),* **41** [6] 589-600 (1948).

22. J.E. Post, "Manganese Oxide Minerals: Crystal Structures and Economic and Environmental Significance," *Proc. Natl. Acad. Sci.,* **96** 3447-54 (1999).

23. G.M. Faulring, "Unit Cell Determination and Thermal Transformations of Nsutite," *Am. Mineral.,* **50** [1] 170-79 (1965).

24. H.E. Swanson, H.F. McMurdie, M.C. Morris, E.H. Evans, and B. Paretzkin, "Standard X-ray Diffraction Powder Patterns," *NBS Monogr. 25,* **11** 95 (1974).

25. D. Jarosch, "Crystal Structure Refinement and Reflectance Measurements of Hausmannite, Mn_3O_4," *Mineral. Petrol.,* **37** [1] 15-23 (1987).

26. H.F. McMurdie, B.M. Sullivan, and F.A. Mauer, "High Temperature X-ray Study of the System Fe_3O_4-Mn_3O_4," *J. Res. Natl. Bur. Stand.,* **45** [1] 35 (1950).

27. F.C.M. Driessens, "Place and Valence of the Cations in Mn_3O_4 and Some Related Manganates," *Inorg. Chim. Acta,* **1** [1] 193-201 (1967).

28. G.M. Faulring, W.K. Zwicker, and W.D. Forgeng, "Thermal Transformations and Properties of Cryptomelane," *Am. Mineral.,* **45** [9] 946-59 (1960).

29. J.D. Scott, "Crystal Structure of a New Mineral, Sohngeite," *Am. Mineral.,* **56** [1/2] 355 (1971).

30. S. Geller, "Crystal Structure of β-Ga_2O_3," *J. Chem. Phys.,* **33** [3] 676-84 (1960).

31. P.G. Casado and I. Rasines, "Crystal Data for the Spinels MGa_2O_4 (M= Mg, Mn)," *Z. Kristallogr.,* **160** [1/2] 33-7 (1982).

32. C.A. Sorrell, "Phase Analysis," pp. 561-63 in Engineered Materials Handbook, Vol. 4, *Ceramics and Glasses.* Edited by S.J. Schneider. ASM International, Materials Park, Ohio, 1991.

33. D. Edwards, T.O. Mason, W. Sinkler, L.D. Marks, K.R. Poeppelmeier, X. Hu, and J.D. Jorgensen, "Tunneled Intergrowth Structures in the Ga_2O_3-In_2O_3-SnO_2 System," *J. Solid State Chem.,* **150** [2] 294-304 (2000).

34. F.A. Cotton, G. Wilkinson, and P.L. Gaus, *Basic Inorganic Chemistry*, 3rd ed.*;* pp. 358-9, 562-4. John Wiley & Sons, New York, 1995.

35. S.J. Li, C. Zheng, and K.C. Lobring, "Refinement of the Crystal Structure of Gallium Oxide Hydroxide, GaO(OH)," *Z. Kristallogr.-New Cryst. Struct.,* **218** [1] 11-2 (2003).

36. M. Mizuno, T. Yamada, and T. Noguchi, "The Liquidous Curve in the System Al_2O_3-Ga_2O_3 as Measured with a Solar Furnace," *Dainippon Yogyo Kyokai Zasshi,* **83** [4] 175-7 (1975).

37. D. Edwards, P.E. Folkins, and T.O. Mason, "Phase Equilibria in the Ga_2O_3-In_2O_3 System," *J. Am. Ceram. Soc.,* **80** [1] 253-57 (1997).

38. V.G. Hill, R. Roy, and E.F. Osborn, "The System Alumina-Gallia-Water," *J. Am. Ceram. Soc.,* **35** [6] 135-42 (1952).

4 Conclusions and Recommendations for Future Work

Low n-value β-gallia rutile intergrowths were not formed in the Ga_2O_3-Al_2O_3-TiO_2 or Ga_2O_3-MnO_2 systems. Suggestions for future work prompted by this study include further analysis of existing data and also proposed changes to processing parameters.

The addition of Al^{3+} decreased the size of the β-gallia and pseudobrookite unit cells as shown by x-ray patterns and lattice parameter calculations. This reduction in the size of the β-gallia component did not stabilize low n-value intergrowths in the Ga_2O_3-Al_2O_3-TiO_2 system, where the lowest stable n-value intergrowth was n = 17. It is apparent that lattice mismatch is not the only reason for instability in this system at the studied temperature.

Future work in this area should include experiments at higher temperatures up to the melting point, because it has been shown previously that lower-n value intergrowths may become stable at higher temperatures. Also, processing methods that would hinder the formation of pseudobrookite in favor of the intergrowth structure should be investigated.

The Ga_2O_3-MnO_2 system has shown interesting behavior and would benefit from further analysis. The addition of a standard to all x-ray diffraction data would give better insight as to how much manganese was actually incorporated into the diaspore structure of α-GaOOH and the β-gallia structure. Also, the location of these dopants, including the existence of any Jahn-Teller distortion could be investigated through Rietveld analysis of X-ray and neutron diffraction data.

The effect of processing parameters on the results should be further investigated. Repeatability experiments would need to be conducted to be sure of processing conditions and resultant compositions. Further TEM analysis of samples would give further insight to the effect of processing parameters on particle morphology and phase composition.

Unknown minor and major phase samples may contain new crystal structures of interest to the battery industry. Further research could give better insight as to the composition of the unknown minor and major phases. In-situ x-ray analysis would give

more reliable information on the evolution of phases with heating. UV-vis spectrometry could give information on the types of bonds present within the sample. Separate experiments involving Ga-O-H and Mn-O-H systems may be helpful in analyzing unknown phases.

Variations on the processing conditions could yield different phases. The hydrothermal system used in this study had a temperature limit of 275ºC, constrained by use of a Teflon sample cup. This temperature can be increased by using a sapphire sample cup, which is commercially available. The pressure limit was about 1800 psi for this system, whereas higher pressures can be attained through a higher strength digestion bomb. Formation of the desired intergrowths requires the formation of β-Ga_2O_3 and β-MnO_2 subunits. Because this work showed that β-MnO_2 could be formed at ~ 225ºC at intermediate pH, and other work[1] has reported that α-GaOOH converts to β-Ga_2O_3 at 300ºC under hydrothermal conditions, higher temperature and high pressure processing conditions should be explored.

1. V.G. Hill, R. Roy, and E.F. Osborn, "The System Alumina-Gallia-Water," *J. Am. Ceram. Soc.,* **35** [6] 135-42 (1952).